



HAL
open science

Arabidopsis CER1-LIKE1 Functions in a Cuticular Very-Long-Chain Alkane-Forming Complex 1

Stéphanie Pascal, Amélie Bernard, Paul Deslous, Julien Gronnier, Ashley Fournier-Goss, Frédéric Domergue, Owen Rowland, Jérôme Joubès

► **To cite this version:**

Stéphanie Pascal, Amélie Bernard, Paul Deslous, Julien Gronnier, Ashley Fournier-Goss, et al.. Arabidopsis CER1-LIKE1 Functions in a Cuticular Very-Long-Chain Alkane-Forming Complex 1. Plant Physiology, 2019, 179 (2), pp.415-432. 10.1104/pp.18.01075 . hal-02368049

HAL Id: hal-02368049

<https://hal.science/hal-02368049v1>

Submitted on 10 Dec 2024

HAL is a multi-disciplinary open access archive for the deposit and dissemination of scientific research documents, whether they are published or not. The documents may come from teaching and research institutions in France or abroad, or from public or private research centers.

L'archive ouverte pluridisciplinaire **HAL**, est destinée au dépôt et à la diffusion de documents scientifiques de niveau recherche, publiés ou non, émanant des établissements d'enseignement et de recherche français ou étrangers, des laboratoires publics ou privés.

Arabidopsis CER1-LIKE1 Functions in a Cuticular Very-Long-Chain Alkane-Forming Complex¹

Stéphanie Pascal,^{a,b} Amélie Bernard,^{a,b} Paul Deslous,^{a,b} Julien Gronnier,^{a,b,2} Ashley Fournier-Goss,^c Frédéric Domergue,^{a,b} Owen Rowland,^c and Jérôme Joubès^{a,b,3,4}

^aUniversité de Bordeaux, Laboratoire de Biogenèse Membranaire, UMR5200, F-33000 Bordeaux, France

^bCNRS, Laboratoire de Biogenèse Membranaire, UMR5200, F-33000 Bordeaux, France

^cDepartment of Biology and Institute of Biochemistry, Carleton University, Ottawa, Ontario K1S 5B6, Canada

ORCID IDs: 0000-0002-9956-6113 (S.P.); 0000-0002-1429-0542 (J.G.); 0000-0002-0183-7000 (F.D.); 0000-0001-5385-450X (J.J.).

Plant aerial organs are coated with cuticular waxes, a hydrophobic layer that primarily serves as a waterproofing barrier. Cuticular wax is a mixture of aliphatic very-long-chain molecules, ranging from 22 to 48 carbons, produced in the endoplasmic reticulum of epidermal cells. Among all wax components, alkanes represent up to 80% of total wax in *Arabidopsis thaliana* leaves. Odd-numbered alkanes and their derivatives are produced through the alkane-forming pathway. Although the chemical reactions of this pathway have been well described, the enzymatic mechanisms catalyzing these reactions remain unclear. We previously showed that a complex made of *Arabidopsis* ECERIFERUM1 (CER1) and CER3 catalyzes the conversion of acyl-Coenzyme A's to alkanes with strict substrate specificity for compounds containing more than 29 carbons. To learn more about alkane biosynthesis in *Arabidopsis*, we characterized the biochemical specificity and physiological functions of a CER1 homolog, CER1-LIKE1. In a yeast strain engineered to produce very-long-chain fatty acids, CER1-LIKE1 interacted with CER3 and cytochrome B5 to form a functional complex leading to the production of alkanes that are of different chain lengths compared to that produced by CER1-containing complexes. Gene expression analysis showed that both CER1 and CER1-LIKE1 are differentially expressed in an organ- and tissue-specific manner. Moreover, the inactivation or overexpression of CER1-LIKE1 in *Arabidopsis* transgenic lines specifically impacted alkane biosynthesis and wax crystallization. Collectively, our study reports on the identification of a further plant alkane synthesis enzymatic component and supports a model in which several alkane-forming complexes with distinct chain-length specificities coexist in plants.

Terrestrial plants have a protective barrier called cuticle that controls the movement of water between the outer cell wall of the epidermis and the atmosphere adjacent to the plant (Shepherd and Wynne Griffiths, 2006; Martin and Rose, 2014; Ingram and Nawrath, 2017). The cuticle consists of cutin, polysaccharides, and associated solvent-soluble lipids called cuticular waxes. Cutin is the main structural component of the cuticular matrix. It consists of polyester of long-chain-polyhydroxy- and epoxyhydroxy-fatty acids cross

linked to each other or via glycerol backbones (Fich et al., 2016). Cuticular waxes are a complex mixture of multiple homologous series of very-long-chain (VLC) aliphatic compounds, as well as nonacyl lipid cyclic components including terpenoids and flavonoids (Buschhaus and Jetter, 2011; Lee and Suh, 2015). The physical and chemical properties of cuticular waxes determine vital functions for plants (Bernard and Joubès, 2013). Besides playing a major role in limiting uncontrolled nonstomatal water loss (Xue et al., 2017), waxes protect plants against ultraviolet radiation and help to minimize deposits of dust, pollen, and other air pollutants (Kunst and Samuels, 2003). In addition, surface wax is believed to play important roles in defense against bacterial and fungal pathogens (Ziv et al., 2018) and participates in a variety of plant-insect interactions (Gorb and Gorb, 2017).

Cuticle biosynthesis can be divided into several distinct metabolic blocks. Initially, the C16:0, C18:0, or C18:1 fatty acids resulting from de novo fatty acid synthesis in the plastids are transferred to the extraplastidial acyl-Coenzyme A (CoA) pool, of which a proportion will be used as precursors for the synthesis of cutin monomers and wax components in epidermal cells. The subsequent generation of the cutin polymer can be divided into five successive steps: fatty acyl-chain oxidation, esterification of oxygenated fatty acyl-chains to the *sn*-2 position of glycerol, intracellular

¹This work was supported by the Ministère de l'Enseignement Supérieur et de la Recherche (doctoral fellowship for A.B. and J.G.), by the Centre National de la Recherche Scientifique, by the Natural Sciences and Engineering Research Council of Canada, and the University of Bordeaux.

²Current address: Institute of Plant and Microbial Biology and Zürich-Basel Plant Science Center, University of Zürich, Zürich, 8008, Switzerland.

³Author for contact: jerome.joubes@u-bordeaux.fr.

⁴Senior author.

The author responsible for distribution of materials integral to the findings presented in this article in accordance with the policy described in the Instructions for Authors (www.plantphysiol.org) is: Jérôme Joubès (jerome.joubes@u-bordeaux.fr).

F.D., O.R., and J.J. designed the experiments; S.P., A.B., P.D., J.G., A.F.-G., F.D., O.R., and J.J. performed the experiments; J.J. conceived the project and wrote the article with contributions of all the authors.

trafficking, export to the cell wall, and extracellular polymerization. Wax aliphatic compounds are usually produced through two different pathways: (1) the alcohol-forming pathway, which yields VLC-fatty alcohols and esters (Rowland et al., 2006; Li et al., 2008), and (2) the alkane-forming pathway leading to the formation of VLC-alkanes and their derivatives, secondary *n*-alcohols and ketones (Greer et al., 2007; Bernard et al., 2012). The two metabolic routes share a pool of precursors consisting of VLC fatty acids (VLCFA), with chain lengths ranging from 22 to 38 carbons, which result from the activity of the endoplasmic reticulum (ER)-associated multienzyme fatty acyl-CoA elongase (FAE) complexes (Haslam and Kunst, 2013). Wax components synthesized within the ER are then transported in a directional manner to the plasma membrane before being secreted to cover the cell wall of epidermal cells facing the external environment (Lee and Suh, 2015).

In the past 30 years, forward genetic analyses using *Arabidopsis thaliana* mutants have provided significant advances in our understanding of wax metabolism. The alcohol- and the alkane-forming pathways are now well described, with identification of the genes involved and functional characterization of most of the corresponding proteins (Lee and Suh, 2015).

The alkane-forming pathway, also called the decarbonylation pathway, produces aldehydes and odd-numbered *n*-alkanes, secondary *n*-alcohols, and ketones. Several *Arabidopsis cer* (*eceriferum*) mutants with a decreased *n*-alkane load have been biochemically characterized (Jenks et al., 1995). The *cer3* mutant shows a dramatic reduction in aldehydes, *n*-alkanes, secondary *n*-alcohols, and ketones (Jenks et al., 1995; Chen et al., 2003; Kurata et al., 2003; Rowland et al., 2007). The *cer1* mutant exhibits a substantial decrease in *n*-alkanes and a near abolition of secondary *n*-alcohols and ketones, accompanied by a slight increase in aldehyde content (Aarts et al., 1995; Jenks et al., 1995; Bourdenx et al., 2011). It has been proposed from these phenotypes that *CER3* encodes a VLCFA reductase producing fatty aldehydes, whereas *CER1* encodes an alkane-forming enzyme, which catalyzes the presumed decarbonylation of fatty aldehydes to *n*-alkanes. We previously showed that *CER1* and *CER3* physically interact in plant cells and the coexpression of the two proteins in an engineered VLCFA-producing yeast revealed that *CER1* and *CER3* act synergistically as a heterodimer complex catalyzing the conversion of VLC-acyl-CoAs to *n*-alkanes, with the intermediate aldehyde likely remaining bound to the complex (Bernard et al., 2012). Further, *n*-alkane biosynthesis is enhanced by the addition of cytochromes B5 (CYTB5s) which presumably mediate electron transfer to the catalytic site of *CER1* (Bernard et al., 2012). Additionally, the overexpression of *CER1* in *Arabidopsis* causes a large increase in *n*-alkanes of chain lengths between 29 and 33 carbon atoms, but not *n*-alkanes of shorter chain lengths, indicating that *CER1* has substrate specificity for compounds with more than

29 carbon atoms (Bourdenx et al., 2011). Moreover, the *cer1-1* mutant shows residual *n*-alkane deposition in leaves (Bourdenx et al., 2011) suggesting that *CER1* is not the sole alkane-forming enzyme in *Arabidopsis*.

We previously showed that *CER1* belongs to a four-member gene family in *Arabidopsis*, in which *CER1-LIKE1* (At1g02190) and *CER1-LIKE2* (At2g37700) are highly similar to *CER1* (At1g02205), whereas *CER1-LIKE3* (At5g28280) is likely a pseudogene (Bourdenx et al., 2011). Among the three *CER1-LIKE* genes, only *CER1-LIKE1* was found to be expressed in *Arabidopsis* tissues (Bourdenx et al., 2011), suggesting that it has a significant role in VLC-alkane biosynthesis. To test this hypothesis, we carried out the characterization of the *CER1-LIKE1* protein in this study.

We show here that *CER1-LIKE1* interacts with *CER3* and *CYTB5-B*, suggesting that it is part of an alkane-forming complex. Furthermore, coexpression of *CER1-LIKE1* and *CER3* in yeast results in VLC-*n*-alkane production, but with chain-length substrate specificity shorter than that of the *CER1/CER3* complex. Moreover, the gene expression patterns of *CER1-LIKE1* along with that of other genes of the alkane-forming pathway were analyzed in the different organs of *Arabidopsis*. We confirmed that *CER1-LIKE1* is highly expressed in reproductive organs, but its expression can be also detected in leaves. Using insertional mutants and overexpression lines, we demonstrate that altered *CER1-LIKE1* activity impacts VLC-*n*-alkane biosynthesis and wax crystallization, thus identifying further diversified enzymatic activity of the plant cuticular alkane-forming pathway.

RESULTS

CER1-LIKE1 Is Part of an Alkane-Forming Complex

We previously showed that *CER1*, *CER3*, and *CYTB5* form an ER-localized complex that catalyzes alkane formation in plant cells (Fig. 1A; Bernard et al., 2012). To test the hypothesis that *CER1-LIKE1* is part of a similar alkane-forming complex, we first studied its subcellular localization by transiently coexpressing RFP-*CER1-LIKE1* with YFP-*CYTB5-B* fusion proteins in *Nicotiana benthamiana* leaves. Confocal microscopy analyses showed that *CER1-LIKE1*, like *CER1*, colocalized with *CYTB5-B* at the ER (Fig. 1A). Next, we tested the physical interactions of *CER1-LIKE1* with *CYTB5-B* and *CER3* using a split-ubiquitin yeast two-hybrid assay with Cub-*CER1-LIKE1* as bait and NubG-*CYTB5-B* and NubG-*CER3* as preys (Cub, C-ubiquitin; Nub, N-ubiquitin; Fig. 1B). Unlike yeast cells coexpressing Cub-*CER1-LIKE1* and NubG (negative control), yeast coexpressing Cub-*CER1-LIKE1* and NubG-*CYTB5-B* or NubG-*CER3* were able to grow on the different selective media and displayed β -galactosidase activity, indicating that *CER1-LIKE1* interacts with *CER3* and *CYTB5-B* and belongs to an alkane-forming complex similar to that of *CER1*. Analyses of the yeast

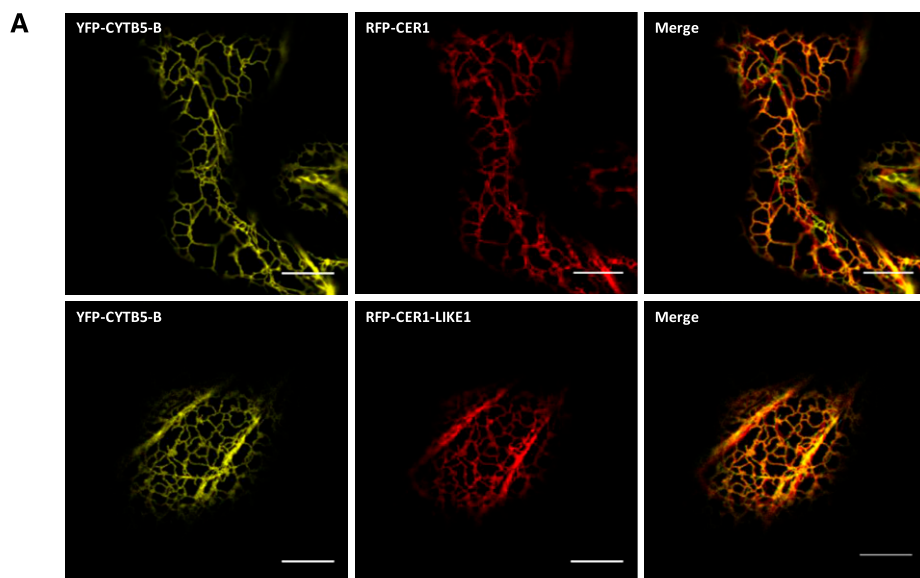
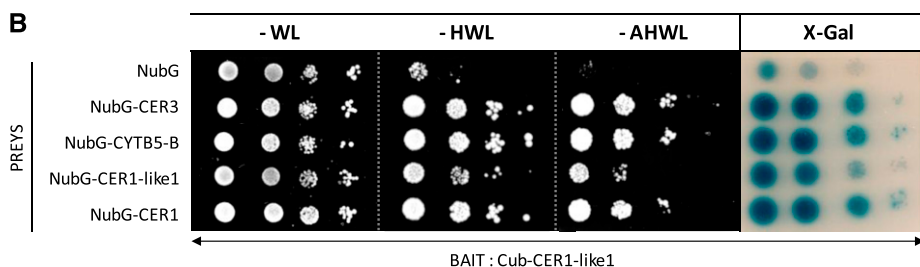


Figure 1. CER1-LIKE1 is part of an alkane-forming complex. A, CER1-LIKE1 physically interacts with CYTB5-B in tobacco cells. Confocal images of tobacco leaves transiently expressing YFP-CYTB5-B and RFP-CER1 or YFP-CYTB5-B and RFP-CER1-LIKE1 as indicated in the figure panels. YFP-CYTB5-B localized to the ER (left), where it colocalized with RFP-CER1 or RFP-CER1-LIKE1 (center), as evident in the merged images (right). Scale bars, 10 μ m. B, CER1-LIKE1 interacts with itself, CER1, CER3, and CYTB5-B in the split ubiquitin yeast two-hybrid system. Yeast cells cotransformed with the different vectors were grown on selective media lacking His, Leu, and Trp (–HWL) or additionally lacking adenine (–AHL) and were tested for β -galactosidase activity (X-gal; OD₆₀₀ yeast cells, left to right, 10⁻¹; 10⁻²; 10⁻³; 10⁻⁴).



coexpressing Cub-CER1-LIKE1 as bait and NubG-CER1 or NubG-CER1-LIKE1 as preys showed that CER1-LIKE1 also interacts with CER1 and with itself, suggesting that it homo- or heterodimerizes in plant cells.

The finding that CER1-LIKE1 physically interacts with CER3 and CYTB5-B suggests that this protein participates in alkane production. To test this hypothesis, MYC-tagged forms of CER1-LIKE1, or CER1 as positive control, were coexpressed with CER3 and CYTB5-B in a yeast strain (INVSur4#) expressing the mutated yeast elongase component SUR4 F262K/K266L, which produces VLCFAs up to 32 carbon atoms (Denic and Weissman, 2007; Bernard et al., 2012). The expression of the different constructs was confirmed by semiquantitative reverse transcription PCR (RT-PCR) and western blot analyses (Fig. 2, A and B). The coexpression of CER1-LIKE1 with CER3 and CYTB5-B led to the production of *n*-alkanes, however to a lesser extent than CER1 (23 ng compared to 81 ng of total hydrocarbons per mg of yeast dry weight). Furthermore, the composition of the purified hydrocarbon fraction was different in cells expressing CER1-LIKE1 compared to CER1 (Fig. 2, C and D). CER1 produces mainly C29 *n*-alkanes (89% of the total hydrocarbons) as well as low amounts of C25, C27, and C31 *n*-alkanes (1.6%, 4.8%, and 4.6% of the total hydrocarbons, respectively). CER1-LIKE1 produces equivalent amounts of C27 and C29 *n*-alkanes (42% and 39% of the total hydrocarbons, respectively)

with a smaller amount of C25 *n*-alkanes (19% of the total hydrocarbons) and traces of C31 *n*-alkanes. Since CER1- and CER1-LIKE1-transformed strains had similar amounts of VLCFAs (Fig. 2E), the different in *n*-alkane profiles obtained results from distinct chain-length specificities of CER1 and CER1-LIKE1 proteins.

Similar to CER1, CER1-LIKE1 possesses a tripartite His cluster. We previously showed that these clusters are essential for the catalytic activity of CER1, where they serve as ligands for a di-iron binding site mediating electron transfer from CYTB5s (Bernard et al., 2012). To test whether His motifs are also required for the activity of CER1-LIKE1, we replaced His 146 (in the first His-rich motif of the tripartite His cluster) by an Ala (CER1-LIKE1 H146A). Yeast coexpressing CER1-LIKE1 H146A with the other components of the complex did not show any *n*-alkane production (Fig. 2, C and D). This demonstrates the functionality of the His-rich cluster of CER1-LIKE1 for the catalytic activity of the enzyme and further supports the idea that CER1-LIKE1 is an alkane-forming enzyme.

Expression Profiling of CER1-LIKE Genes in Arabidopsis Organs

To learn more about the function of CER1-LIKE1 in plants, we analyzed the organ distribution of

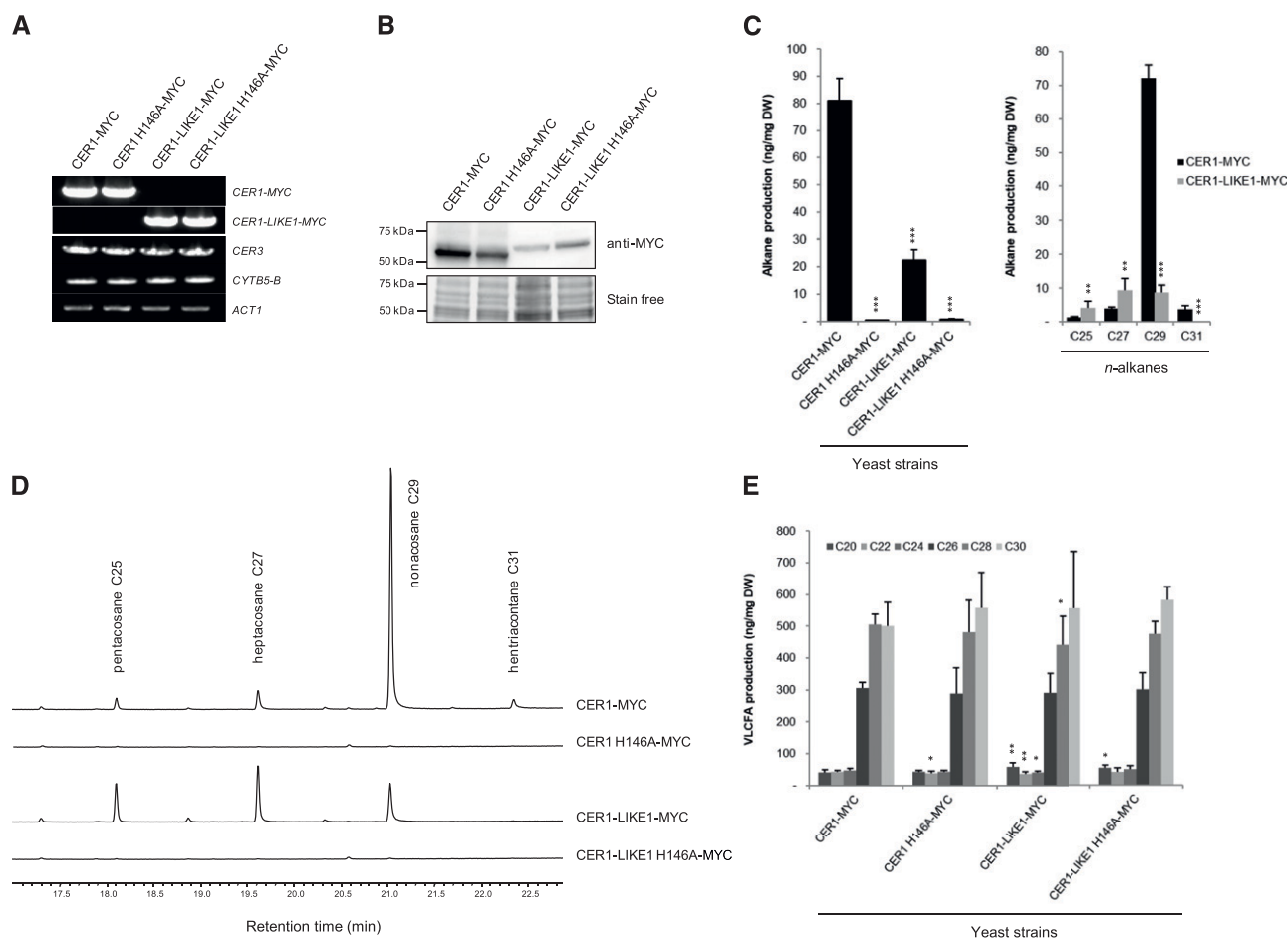


Figure 2. Functional characterization of CER1-LIKE1. A, Semiquantitative analysis of steady-state *CER1-MYC*, *CER1-LIKE1-MYC*, *CER3*, and *CYTB5-B* transcripts (identity indicated on the right) in INVSur4# yeast cotransformed with MYC-tagged wild-type or mutated forms of CER1 or CER1-LIKE1 (indicated at top), *CER3*, and *CYTB5-B*. The yeast *Actin1* (*ACT1*) gene was used as a constitutively expressed control. B, Immunoblot analysis of protein extracts of the different INVSur4# yeast strains expressing MYC-tagged wild-type or mutated forms of CER1 or CER1-LIKE1. Total proteins were imaged using Stain-free technology and used for equal loading control. C, Mean values of total alkanes and individual alkanes of the different INVSur4# yeast strains reported in ng per mg of dry weight (DW). Error bars represent s_D ($n = 4$). Significant differences were assessed by Student's *t* test (* $P < 0.05$; ** $P < 0.01$; *** $P < 0.001$). D, gas chromatography-mass spectrometry traces of the hydrocarbon fractions after separation of total lipid using TLC of the different INVSur4# yeast strains. E, Mean values of VLC fatty acyl (VLCFA) methyl esters of the different INVSur4# yeast strains reported in ng per mg of dry weight (DW). Error bars represent s_D ($n = 4$). Significant differences were assessed by Student's *t* test (* $P < 0.05$; ** $P < 0.01$; *** $P < 0.001$).

CER1-LIKE1 transcripts compared to that of *CER1* and *CER3* by RT-quantitative PCR (qPCR) in seedlings, roots, stems, rosette leaves, flowers, and siliques (Fig. 3A). As previously shown, *CER1* and *CER3* genes showed a typical cuticular wax-associated expression pattern, as they were found to be expressed only in aerial vegetative and reproductive organs. In comparison, we found that *CER1-LIKE1* transcripts were barely detectable in vegetative organs; however, the gene was highly expressed in reproductive organs.

Expression of *CER1-LIKE1* in flowers suggests that the corresponding protein is required for the production of waxes on floral organs or for the synthesis of the aliphatic components of the pollen wall. To explore the

functions of *CER1-LIKE1* during flower development, we analyzed its expression in flowers, collected at different development stages, in comparison to the expression patterns of a set of key genes: *CER1*, *CER3*, *CER2-LIKE2* (also named *CER26-LIKE*), and *FAR2* (also named *MS2*; Fig. 3B). *CER1* and *CER3* are expressed throughout flower development and contribute to cuticle formation of the different floral organs (Kurata et al., 2003; Bourdenx et al., 2011). *CER2-LIKE2* and *FAR2* are mostly expressed in young flower buds, which fits with their role in pollen wall formation by regulating the synthesis of sporopollenin precursors in the tapetal cells (Aarts et al., 1997; Chen et al., 2011; Haslam et al., 2015). We found that, like *CER1* and *CER3*, *CER1-LIKE1* is expressed at every flower

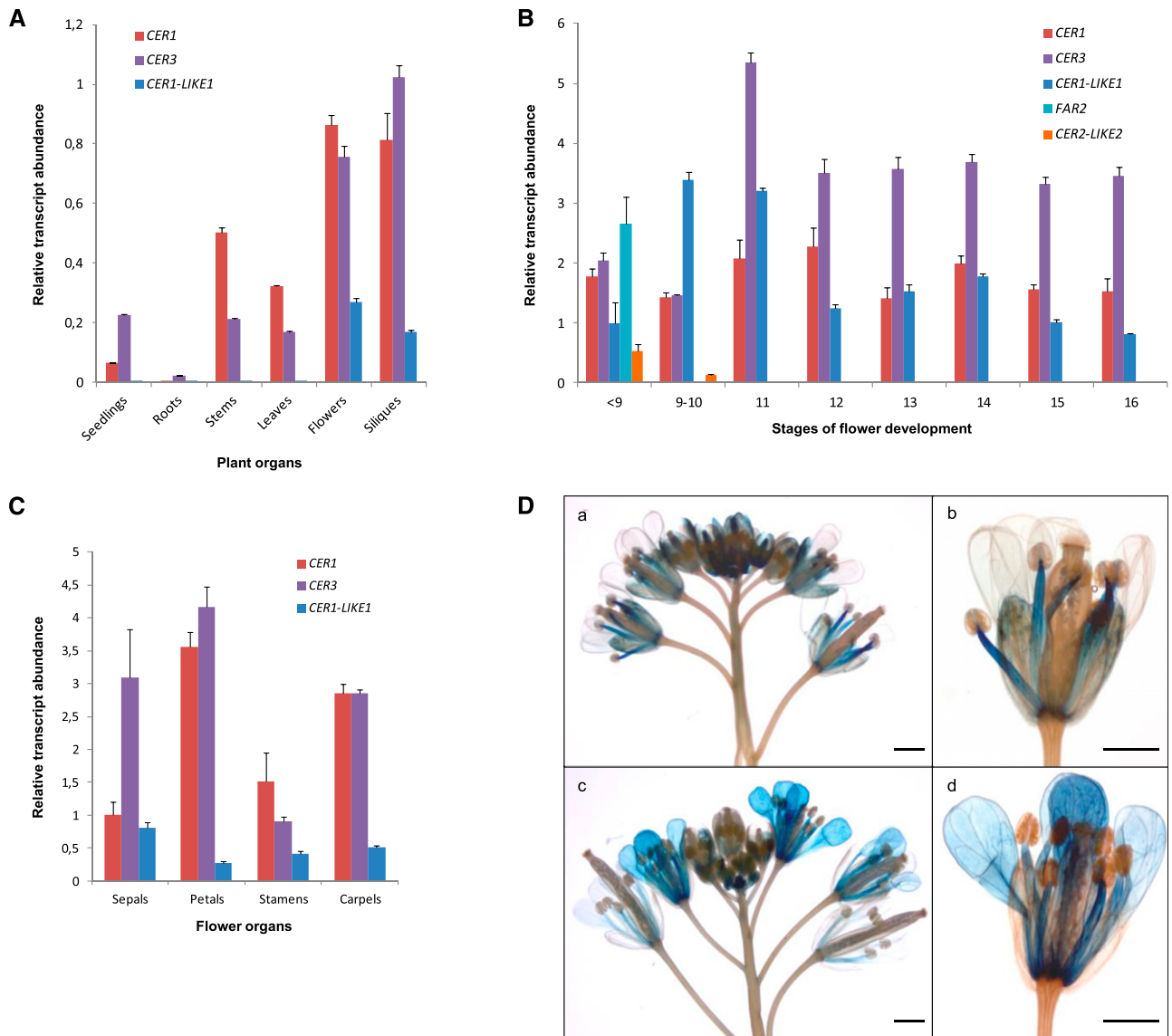


Figure 3. Expression analysis of *CER1-LIKE* gene family in Arabidopsis. **A**, Differential expression analysis of Arabidopsis *CER1*, *CER3*, and *CER1-LIKE1* transcripts in various organs of Arabidopsis. The gene expression level was determined by RT-qPCR analysis. Results are presented as relative transcript abundance. The relative transcript abundance of *ACT2*, *EF-1a*, *eIF-4A-1*, *UBQ10*, and *PP2A* in each sample was determined and used to normalize for differences of total RNA amount. The data represent the means \pm SD of five replicates. Total RNA was isolated from 15-d-old seedlings, roots, stems, leaves, flowers, and siliques. **B**, Differential expression analysis of *CER1*, *CER3*, *CER1-LIKE1*, *FAR2*, and *CER2-LIKE2* genes in Arabidopsis flowers throughout development, following the staging described by Smyth et al. (1990) for early floral development. The relative transcript abundance of *ACT2* and *eIF-4A-1* in each sample was determined and used to normalize for differences of total RNA amount. Results for each gene are presented as transcript abundance compared to expression level of *CER1-LIKE1* at stage <9. The data represent the means \pm SD of three replicates. **C**, Differential expression analysis of *CER1*, *CER3*, and *CER1-LIKE1* genes in Arabidopsis flower organs at stage 14. The relative transcript abundance of *ACT2* and *eIF-4A-1* in each sample was determined and used to normalize for differences of total RNA amount. Results for each gene are presented as transcript abundance compared to expression level of *CER1* in sepals. The data represent the means \pm SD of three replicates. **D**, Spatial expression patterns of the *CER1-LIKE1* (a and b) and *CER1* (c and d) genes in transgenic Arabidopsis plants harboring the *CER1-LIKE1* and *CER1* promoters fused to the *GUS* reporter gene. Promoter activity was visualized through histochemical *GUS* staining on flower buds (a and c, scale bars = 1 mm) and flower at stage 15 (b and d, scale bars = 2 mm).

development stage, suggesting that it is required for cuticular wax biosynthesis on the different floral organs.

To better characterize the distribution of *CER1-LIKE1*, its expression was analyzed in sepals, petals, stamens, and carpels of flowers harvested at stage 14 and compared to that of *CER1* and *CER3* (Fig. 3C). RT-qPCR analyses showed that the three genes are expressed in all four organs. Overall *CER1-LIKE1* shows a weaker expression than *CER1* and *CER3* except in sepals, where it is comparable to the level of *CER1*. The expression patterns of *CER1-LIKE1* and *CER1* were also compared using transgenic Arabidopsis lines expressing the *GUS* reporter gene under the control of either the *CER1-LIKE1* or *CER1* promoter (Fig. 3D). Analyses of *GUS* activity recapitulated results obtained by RT-qPCR. *CER1-LIKE1* promoter-driven *GUS* expression was only detected in flowers and most notably in young carpels, sepals, and filament of anthers but was barely detectable in petals. In contrast, *CER1* was expressed in young carpels, petals, and filament of anthers. Together, these results show that *CER1* and *CER1-LIKE1* have overlapping and differential gene expression distributions in flower organs and throughout development, suggesting that they perform complementary functions in wax biosynthesis in flowers.

Functional Characterization of an Arabidopsis *cer1-like1-1* Mutant

The finding that *CER1-LIKE1* is mostly expressed in reproductive organs suggests that it participates with *CER1* in the formation of *n*-alkanes in flowers. To test this hypothesis, we compared the cuticular wax compositions of *cer1-like1-1* and *cer1* knockout mutants. We selected the *cer1-like1-1* allele (SM_3_23790/CS112237 in Col-0 ecotype), in which the *CER1-LIKE1* gene is disrupted in the first exon (at nucleotide 300 relative to the start codon; Fig. 4A). In the following experiments, the *cer1-like1-1* mutant was compared to the previously reported *cer1-1* mutant (SALK_008544), in which *CER1* is disrupted by a transfer DNA (T-DNA) insertion in the last exon (Bourdenx et al., 2011). Transposon and T-DNA insertions were confirmed by PCR on genomic DNA (Fig. 4B), and inactivation of the genes was confirmed by RT-qPCR analysis in flowers of the different mutants (Fig. 4C).

To compare the activity of *CER1-LIKE1* and *CER1* in the biosynthesis of cuticular waxes, we analyzed the cuticular wax compositions of flowers, stems, and leaves of the following genotypes: wild-type (Col-0), *cer1-1*, and *cer1-like1-1* (Figs. 4 and 5; Tables 1–3).

In flowers, the total wax load of the *cer1-1* mutant was considerably reduced compared to that of wild-type plants (82% decrease; Fig. 4E; Table 1), but not completely abolished like it was in stems (99% decrease; Fig. 5A; Table 2). This decrease was largely due to a reduction of the three major components of flower waxes: the C29 *n*-alkane and its derivatives C29 secondary *n*-alcohol and C29 ketone (91% decrease;

Fig. 4F). The amounts of other components with 29 or more carbons (C31 *n*-alkane, C29, and C31 *iso*-alkanes) were also dramatically decreased in *cer1-1* (73% decrease), whereas the amounts of components with less than 29 carbons (C25 and C27 *n*-alkanes and C27 *iso*-alkane) were less affected (33% decrease). In the *cer1-like1-1* mutant, the wax load was only slightly affected when compared to that of wild-type plants (6% decrease), mainly due to a slight reduction of the *n*-alkane content (Fig. 4E; Table 1). However, whereas the amount of the C29 *n*-alkane was only slightly reduced (8% decreased), the quantities of the C25 and C27 *n*-alkanes and C27 *iso*-alkanes were highly reduced (76% decreased; Fig. 4F). Together, these defects in wax composition suggest that *CER1-LIKE1* is a key component of C25 and C27 alkanes synthesis in flowers, where it could partially complement the activity of *CER1*.

Consistent with an absence of expression of *CER1-LIKE1* in inflorescence stems, the *cer1-like1-1* mutant exhibits no visual phenotype of the inflorescence stem surface compared to that of the *cer1-1* mutant, which exhibits a glossy phenotype and conditional male sterility (Fig. 4D). Furthermore, the loss of *CER1-LIKE1* had no substantial effect on the cuticular wax composition of stems compared to that of wild-type plants, whereas in the *cer1-1* mutant the amount of stem wax was considerably reduced, with production of *n*-alkanes almost abolished (Fig. 5, A and B; Table 2).

The wax load of the *cer1-like1-1* mutant leaves was affected to a small degree when compared to that of wild-type plants (6% decrease) due to slight reductions of C27, C29, C31, and C33 *n*-alkane content (9% decrease in total; Fig. 5, C and D; Table 3). We found that substantial amounts of *n*-alkanes are still produced in the *cer1-1* leaves (16%), with the amounts of the three major *n*-alkanes of leaf waxes, C29, C31, and C33 *n*-alkanes, being highly reduced (Fig. 5D), whereas the amounts of other *n*-alkanes were not much affected, suggesting that the alkane-forming activity of *CER1-LIKE1* generates the remaining *n*-alkanes. Our expression results showed that *CER1-LIKE1* is barely detectable in leaves of wild-type plants (Fig. 3A). Further semiquantitative RT-PCR analyses confirmed that *CER1-LIKE1* transcripts were detected at very low level in leaves of wild-type plants compared to that of *CER1* and *CER3* and that its expression seems to be enhanced in leaves of the *cer1-1* mutant (Fig. 5E).

Ectopic Expression of *CER1-LIKE1* in Stems and Leaves Alters Cuticular Wax Biosynthesis

To further characterize the function of *CER1-LIKE1* in cuticular wax metabolism, we generated Arabidopsis overexpression lines harboring the *CER1-LIKE1* coding sequence along with a MYC tag coding sequence fused at the 3' end of the coding sequence, under the control of the *Cauliflower mosaic virus 35S* promoter. *CER1-LIKE1* was overexpressed in the wild-type (Col-0) background

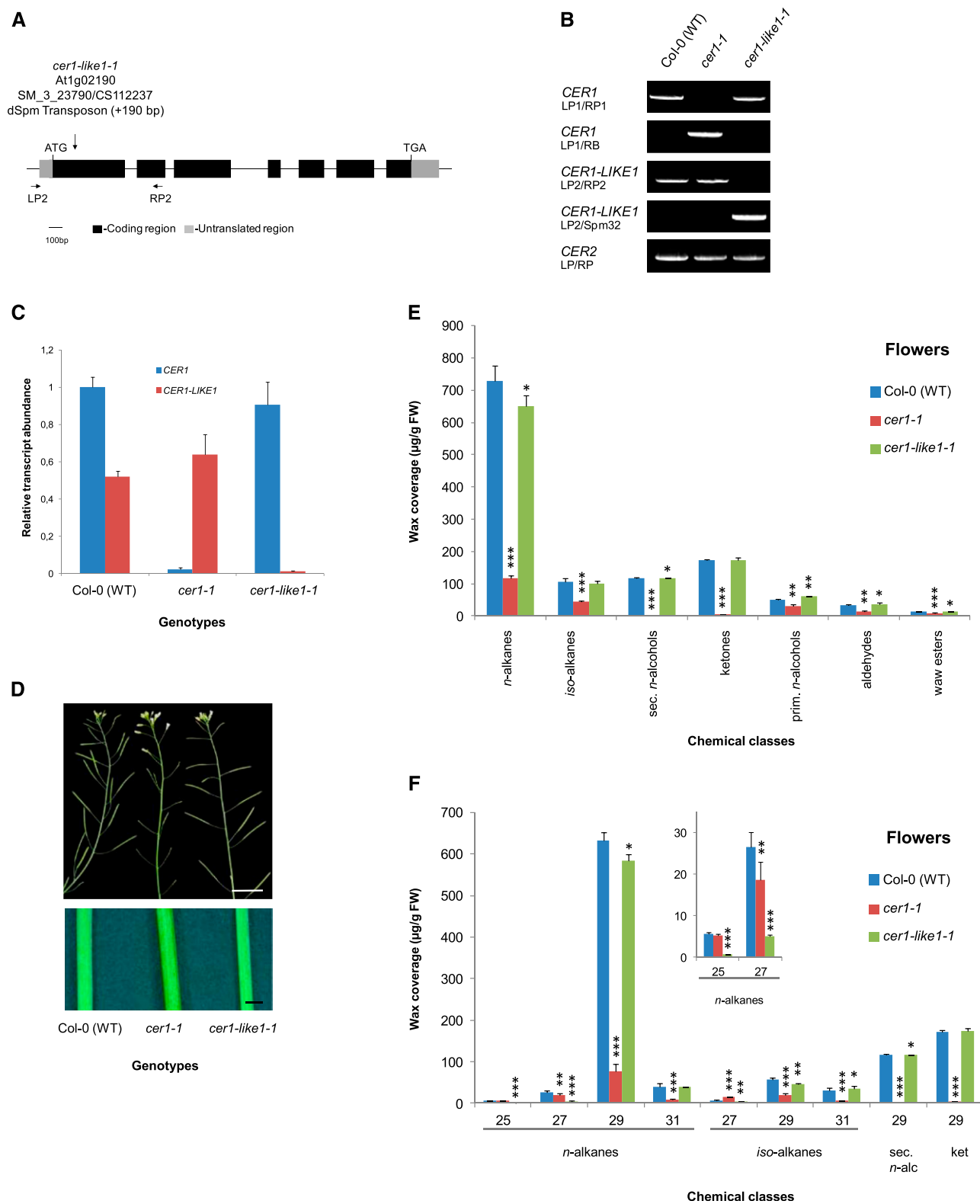


Figure 4. Characterization of *cer1-like1* and *cer1* mutants, including flower wax composition. A, Schematic of *CER1-LIKE1* gene structure indicating the position of the transposon in the mutant *cer1-like1-1* allele. Dark boxes indicate exons, black lines indicate introns, and gray boxes indicate 5'- and 3'-untranslated regions. The arrows underneath the gene structure are the positions of convergent primers (LP2 and RP2) used for PCR on genomic DNA. B, PCR on genomic DNA of wild-type (Col-0) plants, *cer1*, and *cer1-like1-1* mutants. Amplification of the *CER2* gene was used as a positive control. C, RT-qPCR analysis of *CER1-LIKE1* and

as well as in the *cer1-1* background and compared to *CER1Ox* lines (Bourdenx et al., 2011). RT-qPCR analyses of gene expression in stems and leaves and western blot analyses confirmed the overexpression of *CER1-LIKE1* or *CER1* in the different genetic backgrounds (Fig. 6, A and B).

The effects of *CER1-LIKE1* overexpression on wax biosynthesis were assessed by analyzing the cuticular wax compositions of leaves and stems of the different lines (wild-type [Col-0], *CER1-LIKE1Ox*, *CER1Ox*, and *cer1-1:CER1-LIKE1Ox*; Fig. 6; Tables 2 and 3).

In leaves, *CER1-LIKE1* overexpression in the *cer1-1* background partially rescued the defective wax biosynthesis of the mutant, leading to a strong increase of the wax load (64% increase) similar to that found in the *CER1-LIKE1Ox* and *CER1Ox* lines (76% and 111% increases, respectively; Fig. 6C; Table 3). This was largely manifested as increases in the *n*-alkane amounts (90%, 128%, and 166% increases in *cer1-1:CER1-LIKE1*, *CER1-LIKE1Ox*, and *CER1Ox*, respectively). We also noted a large increase of *iso*-alkane amounts in these lines (699%, 1,187%, and 1,156% increases, respectively) characterized by increases in the C29 and C31 *iso*-alkane amounts (Fig. 6D). In contrast, other wax components, namely primary *n*-fatty alcohols and fatty aldehydes, were not significantly affected. Analysis of the chain-length composition of the odd-carbon-numbered *n*-alkanes revealed differences between the *CER1*- and *CER1-LIKE1*-overexpressing lines (Fig. 6D). While the overexpression of *CER1* causes a large increase of C31 and C33 *n*-alkanes (154% and 426% increases), the overexpression of *CER1-LIKE1* led to very large increases of C25 and C27 *n*-alkanes only (1,314% and 1657% increases, respectively, in *CER1-LIKE1Ox* and 1,225% and 1,408% increases, respectively, *cer1-1:CER1-LIKE1Ox*).

In stems, the overexpression of *CER1-LIKE1* almost restored wax production in the *cer1-1* background (88% of the waxes of wild-type plants; Table 2) and showed a similar pattern to the *CER1-LIKE1Ox* line (Fig. 6E). Yet wax composition was greatly affected compared to that of wild-type and *CER1Ox* lines. Indeed, *cer1-1:CER1-LIKE1Ox* and *CER1-LIKE1Ox* lines showed large increases in C25 and C27 *n*-alkane amounts (5,386% and 1,462%, and 4,406% and 1718% increases, respectively),

which caused a 32% increase in *n*-alkanes in the *CER1-LIKE1Ox* line (Fig. 6, E and F; Table 2). Despite this increase, the secondary *n*-alcohol and ketone levels were slightly decreased compared to that in wild-type plants (around 38% and 27% decreases, respectively). Finally, primary *n*-fatty alcohol and aldehyde amounts were only slightly altered in this line compared to that in wild-type plants.

Despite the rescue of wax synthesis by overexpressing *CER1-LIKE1* in the *cer1-1* mutant, the transgenic line still displayed the characteristic visual phenotype of the mutant, i.e. a bright green stem and conditional male sterility, which is usually associated with a depletion of wax crystals in *cer* mutants (Fig. 7A). The glossy stem phenotype was also observed in the *CER1-LIKE1Ox* line (Fig. 7A), which was nevertheless fertile. To analyze the morphology of epicuticular wax crystals, we used cryoscanning electron microscopy to visualize the surfaces of young stems in the different lines (Fig. 7B). Wild-type and *cer1-like1-1* stems showed a typical mixture of platelets, joint-plates, and polygonal rodlets protruding from the ubiquitous wax film. As previously shown, the surface of the *cer1-1* mutant was completely devoid of crystals, whereas the surface of the *CER1Ox* stem was enriched in polygonal rodlets. In contrast, the surface the *CER1-LIKE1Ox* and *cer1-1:CER1-LIKE1Ox* stems showed a totally different crystalline organization, with platelets and occasional polygonal rodlets arising from an underlying amorphous layer.

DISCUSSION

CER1-LIKE1 Encodes an Alkane-Forming Enzyme

The synthesis of VLC *n*-alkanes is a major process in the production of cuticular waxes, with *n*-alkanes accounting for 70% to 80% of the wax compounds in *Arabidopsis* leaves (Bernard and Joubès, 2013). In reproductive organs, the alkanes produced can be partially converted into derivatives such as ketones or secondary *n*-alcohols, and all these compounds represent between 80% and 90% of the total wax load depending on the organ (Buschhaus and Jetter, 2012).

Figure 4. (Continued.)

CER1 gene expression in flowers of the different lines compared to that in wild-type plants as indicated above. The relative transcript abundance of *ACT2* and *elf-4A-1* was determined in each sample and used to normalize for differences of total RNA amount. Results for each gene are presented as transcript abundance compared to the expression level of *CER1* in wild-type (Col-0) plants. The data represent the means \pm SD of three replicates. D, Stems from 6-week-old plants of the *cer1-1* mutant showing glossy and sterility phenotypes compared with that of the wild-type (Col-0) and the *cer1-like1-1* mutant (top, scale bar = 1 cm; bottom, scale bar = 1 mm). E, Cuticular wax compound composition, by chemical class, of flowers of wild-type (Col-0), *cer1-1*, and *cer1-like1-1* lines. Amounts of components are expressed as $\mu\text{g}\cdot\text{g}^{-1}$ of fresh weight (FW). The data represent the means \pm SD of three replicates (sec. *n*-alcohols, secondary fatty alcohols; prim. *n*-alcohols, primary fatty alcohols). Significant differences were assessed by Student's *t* test (**P* < 0.05; ***P* < 0.01; ****P* < 0.001). F, Carbon-chain-length distribution within the major cuticular compound classes of flowers of wild-type (Col-0), *cer1-1*, and *cer1-like1-1* lines. Amounts of components are expressed as $\mu\text{g}\cdot\text{g}^{-1}$ of fresh weight. Each wax constituent is designated by carbon chain length and is labeled by chemical class along the x axis (sec. *n*-alc, secondary fatty alcohols, ket, fatty ketones). The data represent the means \pm SD of three replicates. Significant differences were assessed by Student's *t* test (**P* < 0.05; ***P* < 0.01; ****P* < 0.001).

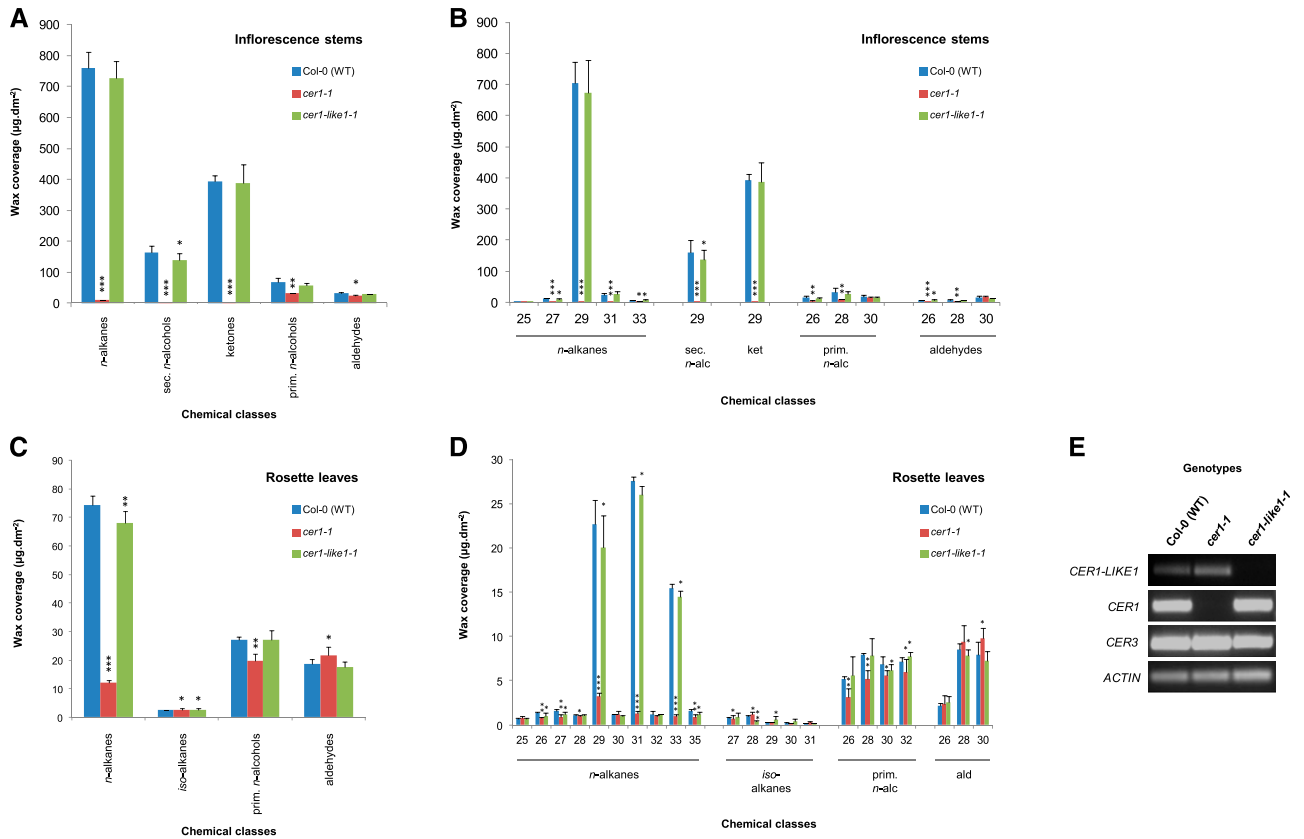


Figure 5. Wax composition of stems and leaves of *cer1* and *cer1-like1* mutants. A, Cuticular compound class composition of stems of wild-type (Col-0), *cer1-1*, and *cer1-like1-1* lines. Amounts of components are expressed as $\mu\text{g}\cdot\text{dm}^{-2}$. The data represent the means \pm SD of three replicates (sec. *n*-alcohols, secondary fatty alcohols; prim. *n*-alcohols, primary fatty alcohols). Significant differences were assessed by Student's *t* test ($*P < 0.05$; $**P < 0.01$; $***P < 0.001$). B, Carbon-chain-length distribution within the major cuticular wax compound classes of stems of wild-type (Col-0), *cer1-1*, and *cer1-like1-1* lines. Amounts of components are expressed as $\mu\text{g}\cdot\text{dm}^{-2}$. Each wax constituent is designated by carbon chain length and is labeled by chemical class along the x axis (ket, fatty ketones). The data represent the means \pm SD of three replicates. Significant differences were assessed by Student's *t* test ($*P < 0.05$; $**P < 0.01$; $***P < 0.001$). C, Cuticular wax compound class composition of leaves of wild-type (Col-0), *cer1-1*, and *cer1-like1-1* lines. Amounts of components are expressed as $\mu\text{g}\cdot\text{dm}^{-2}$. The data represent the means \pm SD of three replicates. Significant differences were assessed by Student's *t* test ($*P < 0.05$; $**P < 0.01$; $***P < 0.001$). D, Carbon-chain-length distribution within the major cuticular compound classes of leaves of wild-type (Col-0), *cer1-1*, and *cer1-like1-1* lines. Amounts of components are expressed as $\mu\text{g}\cdot\text{dm}^{-2}$. Each wax constituent is designated by carbon chain length and is labeled by chemical class along the x axis (ald, fatty aldehydes). The data represent the means \pm SD of three replicates. Significant differences were assessed by Student's *t* test ($*P < 0.05$; $**P < 0.01$; $***P < 0.001$). E, Semiquantitative RT-PCR analysis of *CER1-LIKE1*, *CER1*, and *CER3* gene expression in young leaves of *cer1-1* and *cer1-like1-1* mutants compared to wild-type plants as indicated above. The relative transcript abundance of *ACT2* in each sample was determined to equal loading of total RNA amount.

Furthermore, recent advances in analytical methods showed that methyl branched alkanes and alkenes are also important components of cuticular waxes in *Arabidopsis* and other species (Busta et al., 2017; Busta and Jetter, 2017).

The biosynthetic pathway of cuticular alkanes has been fairly well described in several species (Bernard et al., 2012; Zhou et al., 2013; Wang et al., 2015a, 2015b). The VLC acyl-CoAs produced in the epidermal cells by the fatty acid elongation complexes are converted into

Table 1. Cuticular Wax Composition of Flowers of *Arabidopsis* Wild-Type, *cer1-1*, and *cer1-like1-1* lines.

Mean values ($\mu\text{g}\cdot\text{g}^{-1}$ of fresh weight) of total wax loads and amounts of individual compound classes are given \pm sbs ($n = 3$). The sums include shorter chain-length constituents not presented in Figure 4.

Plant	Total Load	<i>n</i> -Alkanes	<i>iso</i> -Alkanes	Sec. <i>n</i> -Alcohols	Ketones	Prim. <i>n</i> -Alcohols	Aldehydes	Esters
Col-0 (WT)	1220.4 \pm 39.9	729.6 \pm 45.4	107.1 \pm 11.0	117.5 \pm 2.3	171.6 \pm 5.3	49.4 \pm 2.3	31.7 \pm 3.4	13.5 \pm 0.6
<i>cer1-1</i>	217.2 \pm 12.6	116.3 \pm 9.3	43.8 \pm 2.9	1.0 \pm 0.3	4.0 \pm 0.3	29.5 \pm 5.3	13.3 \pm 3.0	9.3 \pm 0.5
<i>cer1-like1</i>	1147.1 \pm 43.9	649.7 \pm 33.6	100.8 \pm 8.3	115.6 \pm 1.6	172.8 \pm 7.3	60.2 \pm 1.4	35.1 \pm 7.8	12.9 \pm 0.5

Table 2. Cuticular Wax Composition of Inflorescence Stems of *Arabidopsis* Wild-Type, *cer1-1*, *cer1-like1-1*, *CER1-LIKE1Ox*, *CER1Ox*, and *cer1-1:CER1-LIKE1Ox* lines.

Mean values ($\mu\text{g}\cdot\text{dm}^{-2}$) of total wax loads and amounts of individual compound classes are given \pm sds ($n = 3$). The sums include shorter chain-length constituents not presented in Figures 5 and 6.

Plant	Total Load	<i>n</i> -Alkanes	Sec. <i>n</i> -Alcohols	Ketones	Prim. <i>n</i> -Alcohols	Aldehydes
Col-0 (WT)	1 415.0 \pm 81.9	759.7 \pm 52.7	163.9 \pm 20.6	392.3 \pm 21.2	68.4 \pm 13.4	30.7 \pm 4.5
<i>cer1-1</i>	66.1 \pm 4.8	9.7 \pm 1.5	1.0 \pm 0.2	0.7 \pm 0.1	30.9 \pm 1.9	23.9 \pm 3.0
<i>cer1-like1</i>	1 339.9 \pm 71.9	726.8 \pm 54.1	139.6 \pm 20.4	388.2 \pm 61.0	56.2 \pm 7.8	29.0 \pm 1.1
<i>CER1-LIKE1Ox</i>	1 475.5 \pm 74.2	1 006.3 \pm 65.1	114.3 \pm 9.8	286.4 \pm 46.3	54.9 \pm 3.3	13.6 \pm 2.0
<i>CER1Ox</i>	1 328.4 \pm 78.7	758.6 \pm 83.1	120.7 \pm 16.9	353.0 \pm 40.0	71.8 \pm 13.6	24.2 \pm 2.0
<i>cer1:CER1-LIKE1Ox</i>	1 183.7 \pm 22.9	757.7 \pm 22.1	75.3 \pm 2.5	284.0 \pm 7.1	44.8 \pm 0.7	21.8 \pm 1.8

n-alkanes by the CER1/CER3 complex. The set of data collected on these two enzymes suggests that CER3 catalyzes the reduction of VLC-acyl-CoA into aldehydes, which, remaining potentially bound to the complex, are decarbonylated by CER1 into *n*-alkanes. The stem waxes of the *Arabidopsis cer1-1* mutant show a substantial reduction in the *n*-alkanes, whereas significant quantities of these compounds still accumulate in leaves or flowers (Bourdenx et al., 2011). This result strongly suggests that another alkane synthase activity exists in epidermal cells that is responsible for the synthesis of the remaining *n*-alkanes. Among other members of the *CER1* gene family, only *CER1-LIKE1* is significantly expressed, most notably in reproductive organs as well as in leaves, albeit at a very low level (Bourdenx et al., 2011). Our data presented here demonstrate that *CER1-LIKE1* is part of the VLC-alkane-forming pathway: (1) the synthesis of *n*-alkanes is partially prevented in leaves and flowers of the *cer1-like1-1* mutant, whereas overexpression of *CER1-LIKE1* causes a significant increase of these compounds in leaves and stems; (2) *CER1-LIKE1*, like *CER1*, is localized to the ER and physically interacts with all components previously associated with alkane formation, i.e. *CER1*, *CER3*, and *CYTB5*; (3) coexpression of *CER1-LIKE1* with *CER3* and *CYTB5* in VLCFA-producing yeast yields VLC-*n*-alkanes.

Several *n*-Alkane-Forming Complexes Coexist in *Arabidopsis*

Comparison of *n*-alkane profiles in transgenic yeast, in the *cer1-1* and *cer1-like1-1* mutants and in *CER1Ox* and *CER1-LIKE1Ox* transgenic plants suggests that *CER1* and *CER1-LIKE1* have differing chain-length substrate

specificities. While *CER1* is mostly associated with the production of *n*-alkanes with 29 or more carbon atoms, *cer1-like1-1* shows stronger defects in the synthesis of compounds with 25 and 27 carbon atoms. Further, when *CER1-LIKE1* is overexpressed in wild-type plants or in the *cer1-1* mutant, a significant increase of *n*-alkanes with 25 and 27 carbon atoms is observed in leaves and stems. Nonetheless, *n*-alkanes with 29 and more carbon atoms are increased in these overexpressing lines, even in the absence of *CER1* activity in the *cer1-1* mutant, suggesting that *CER1-LIKE1* is also capable of catalyzing the synthesis of these components, but less efficiently than *CER1*. The activity of *CER1-LIKE1* can thus explain the residual production of *n*-alkanes from 29 up to 35 carbon atoms found in *cer1-1* leaves. Based on these data, we propose that at least two alkane-forming complexes coexist in *Arabidopsis*, potentially in the same tissue, including specific flower organs and leaves: a complex driven by *CER1-LIKE1*, specific for the synthesis of alkanes from 25 to 29 carbon atoms, and a complex driven by *CER1*, responsible for the synthesis of alkanes with 29 or more carbon atoms. Because *CER3* is involved in alkane formation in both complexes, our results further indicate that the substrate specificity of the complexes is carried by the *CER1* and *CER1-LIKE1* proteins and not by the *CER3* partner. Our analyses also revealed that the waxes of *cer1-1* and *cer1-like1-1* flowers are deficient in methyl-branched alkanes. Furthermore, *CER1-LIKE1Ox* together with *CER1Ox* lines showed a substantial accumulation of iso-branched alkanes in leaves, where they are normally only found in trace amounts, suggesting that both enzymes are able to produce methyl alkanes from methyl VLCFAs. These data confirmed the hypothesis of Busta and Jetter (2017), who suggested that the alkane-forming

Table 3. Cuticular Wax Composition of Rosette Leaves of *Arabidopsis* Wild-Type, *cer1-1*, *cer1-like1-1*, *CER1-LIKE1Ox*, *CER1Ox*, and *cer1-1:CER1-LIKE1Ox* lines.

Mean values ($\mu\text{g}\cdot\text{dm}^{-2}$) of total wax loads and amounts of individual compound classes are given \pm sds ($n = 3$). The sums include shorter chain-length constituents not presented in Figures 5 and 6.

Plant	Total Load	<i>n</i> -Alkanes	iso-Alkanes	Prim. <i>n</i> -Alcohols	Aldehydes
Col-0 (WT)	122.7 \pm 5.1	74.4 \pm 3.2	2.5 \pm 0.2	27.1 \pm 1.0	18.7 \pm 1.5
<i>cer1-1</i>	56.1 \pm 4.0	12.0 \pm 0.9	2.7 \pm 0.4	19.8 \pm 2.3	21.6 \pm 3.1
<i>cer1-like1</i>	115.3 \pm 11.7	68.0 \pm 4.1	2.6 \pm 0.6	27.2 \pm 3.3	17.6 \pm 2.0
<i>CER1-LIKE1Ox</i>	215.5 \pm 11.1	169.8 \pm 2.3	17.1 \pm 0.5	19.2 \pm 2.2	9.4 \pm 1.5
<i>CER1Ox</i>	259.2 \pm 13.7	198.4 \pm 10.5	16.7 \pm 1.8	31.0 \pm 1.2	13.2 \pm 1.6
<i>cer1:CER1-LIKE1Ox</i>	201.1 \pm 12.8	141.5 \pm 2.7	10.9 \pm 1.1	31.9 \pm 5.1	16.9 \pm 2.5

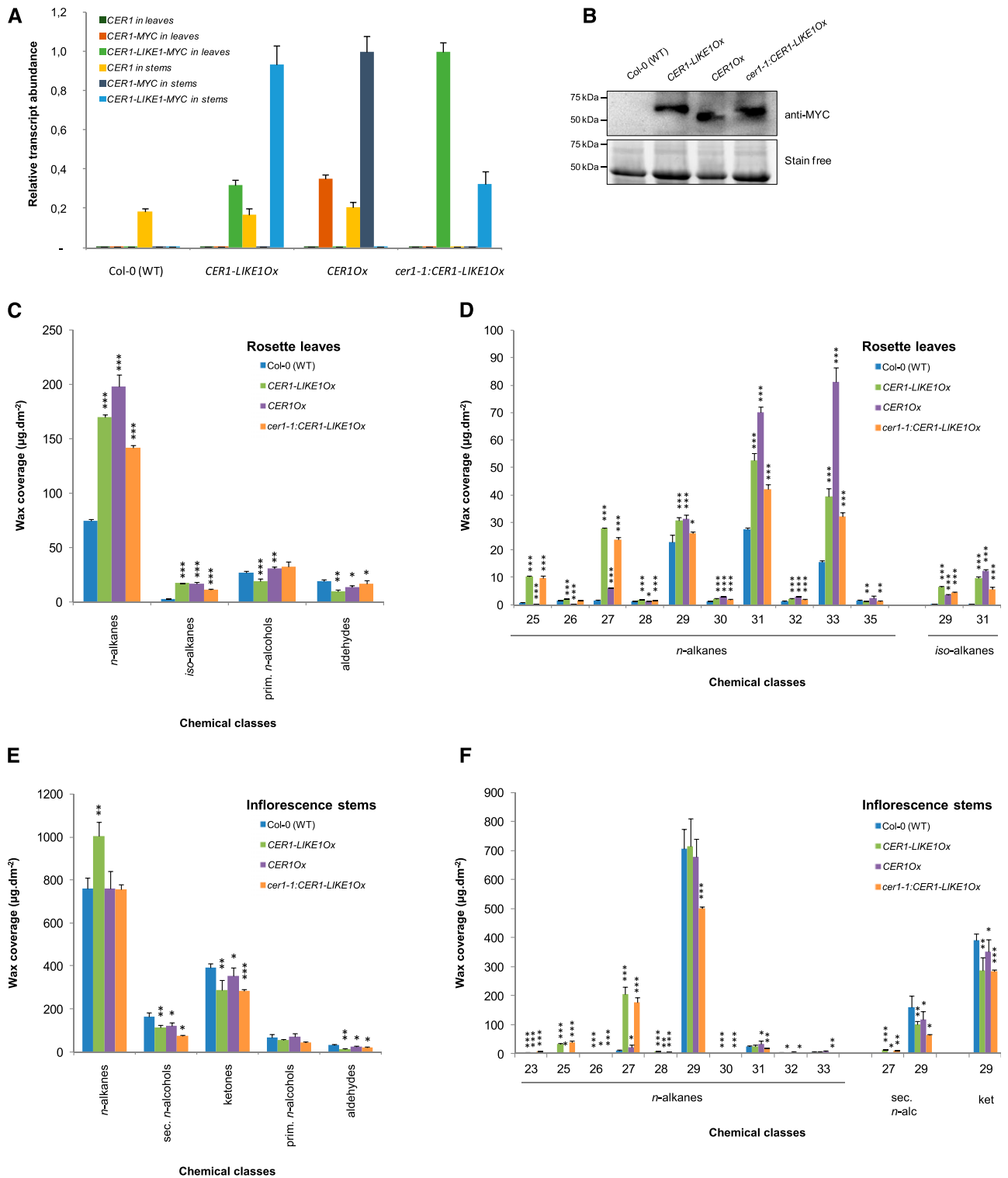


Figure 6. Molecular and biochemical characterization of *CER1-LIKE1* overexpressing plants. **A**, RT-qPCR analysis of *CER1-LIKE1* and *CER1* gene expression in leaves and stems of the different overexpressing lines *CER1-LIKE1Ox*, *CER1Ox*, and *cer1-1:CER1-LIKE1Ox* compared to wild-type plants as indicated above. The relative transcript abundance of *ACT2* and *eIF-4A-1* in each sample was determined and used to normalize for differences of total RNA amount. Results for each gene are presented as transcript abundance compared to maximal expression level in leaves and stems, respectively. The data represent the means \pm SD of three replicates. **B**, Immunoblot analysis of protein extracts of the different lines expressing MYC-tagged forms of CER1 or CER1-LIKE1 compared to wild-type plants as indicated above. Total proteins were imaged using Stain-free technology and used

complexes could accept branched acyl-CoA substrates to form branched alkanes.

Our results indicate that several *n*-alkane synthesis complexes are required to carry out the production of the very broad range of chain lengths in alkanes found in plants, from 25 up to 37 carbon atoms in leaves of Arabidopsis, for example (Bernard and Joubès, 2013; Hegebarth et al., 2017). A variety of other organisms such as bacteria, yeasts, fungi, insects, and microalgae can convert fatty acids into hydrocarbons; nevertheless, enzymes involved in alka(e)ne biosynthesis are not conserved across kingdoms, and a wide variety of pathways for hydrocarbon biosynthesis have been identified in recent years (Fu et al., 2015; Jiménez-Díaz et al., 2017). To our knowledge, only plants seem to have evolved multiple alkane-forming complexes with different chain-length substrate specificities to produce *n*-alkanes with a broad range of chain lengths (Fig. 8). Indeed, insects, which also produce a large spectrum of hydrocarbons (from C21 to C37), convert VLC-acyl-CoA into VLC-alka(e)nes by the sequential activities of two unique enzymes, an acyl-CoA reductase, and an insect-specific P450 oxidative decarbonylase (CYP4G; Qiu et al., 2012). In cyanobacteria, acyl-ACPs are converted into alkanes (mainly C15 and C17) through the acyl-ACP reductase/aldehyde deformylating oxygenase pathway with coproduction of formate instead of CO (Schirmer et al., 2010). Recently, it has been shown that some microalgae are able to produce alka(e)nes (mainly C15, C17, C17:1) due to the activity of a unique fatty acid photodecarboxylase catalyzing the decarboxylation of free fatty acids to alka(e)nes (Sorigué et al., 2016, 2017).

Enzymes with Distinct Substrate Chain-Length Specificities Are Present in Each Metabolic Block Producing Waxes in Arabidopsis

Wax biosynthesis in Arabidopsis relies on three distinct metabolic blocks: the elongation pathway, the alcohol-forming pathway, and the alkane-forming pathway. These biosynthetic routes produce aliphatic compounds with a great range of chain lengths, ranging

from 22 up to 38 carbon atoms. In the elongation pathway, multiple FAE complexes, each with distinct chain-length specificity, perform sequential reactions to produce the broad chain-length range of VLCFAs found in plants (Haslam and Kunst, 2013). Each elongation cycle catalyzes four successive enzymatic activities generating an acyl-chain extended by two carbons. Three of these activities are encoded by single genes in the Arabidopsis genome (β -ketoacyl-CoA reductase, β -hydroxyacyl-CoA dehydratase, and enoyl-CoA reductase); the encoded enzymes have a broad substrate specificity and are shared by all FAE complexes (Zheng et al., 2005; Bach et al., 2008; Beaudoin et al., 2009). In contrast, the β -ketoacyl-CoA synthase activity of the FAE complex is encoded by 21 genes in Arabidopsis (Joubès et al., 2008; Guo et al., 2016), and the characterization of several KCS activities showed that the chain-length specificity of distinct FAE complexes is carried by its KCS subunit (Haslam and Kunst, 2013). Similarly, in the alcohol-forming pathway, which primarily yields VLC-primary *n*-alcohols from VLC-acyl-CoAs (Rowland and Domergue, 2012), four ER-associated fatty acyl reductases (FARs) with distinct acyl chain-length and chain-saturation substrate specificities have been functionally characterized and are able to reduce acyl-CoAs from 18 up to 30 carbon atoms (Rowland et al., 2006; Domergue et al., 2010). For the alkane-forming pathway, leading to the formation of VLC-*n*-alkanes and their derivatives (Greer et al., 2007; Bernard et al., 2012), our present data show that CER1 and CER1-LIKE1 have different acyl chain-length specificities. Altogether, these studies indicate that, in the three major metabolic blocks involved in wax biosynthesis in Arabidopsis, multigenic families encode for enzymes catalyzing the same reaction but with different chain-length specificities leading to the synthesis of aliphatic compounds with a great range of chain lengths.

Crystallization of Epicuticular Waxes

Little is known about the specific contribution of each wax components in the formation of wax crystals

Figure 6. (Continued.)

for equal loading control. C, Cuticular wax composition, by chemical class, of leaves of wild-type (Col-0), *CER1-LIKE1Ox*, *CER1OX*, and *cer1-1:CER1-LIKE1Ox* lines. Amounts of components are expressed as $\mu\text{g}\cdot\text{dm}^{-2}$. The data represent the means \pm SD of three replicates (prim. *n*-alcohols, primary fatty alcohols). Significant differences were assessed by Student's *t* test (* $P < 0.05$; ** $P < 0.01$; *** $P < 0.001$). D, Carbon-chain-length distribution within the major cuticular compound classes of leaves of wild-type (Col-0), *CER1-LIKE1Ox*, *CER1OX*, and *cer1-1:CER1-LIKE1Ox* lines. Amounts of components are expressed as $\mu\text{g}\cdot\text{dm}^{-2}$. Each wax constituent is designated by carbon chain length and is labeled by chemical class along the x axis. The data represent the means \pm SD of three replicates. Significant differences were assessed by Student's *t* test (* $P < 0.05$; ** $P < 0.01$; *** $P < 0.001$). E, Cuticular compound composition, by chemical class, of stems of wild-type (Col-0), *CER1-LIKE1Ox*, *CER1OX*, and *cer1-1:CER1-LIKE1Ox* lines. Amounts of components are expressed as $\mu\text{g}\cdot\text{dm}^{-2}$. The data represent the means \pm SD of three replicates. Significant differences were assessed by Student's *t* test (* $P < 0.05$; ** $P < 0.01$; *** $P < 0.001$). F, Carbon-chain-length distribution within the major cuticular compound classes of stems of wild-type (Col-0), *CER1-LIKE1Ox*, *CER1OX*, and *cer1-1:CER1-LIKE1Ox* lines (sec. *n*-alc, secondary fatty alcohols). Amounts of components are expressed as $\mu\text{g}\cdot\text{dm}^{-2}$. Each wax constituent is designated by carbon chain length and is labeled by chemical class along the x axis (ket, fatty ketones). The data represent the means \pm SD of three replicates. Significant differences were assessed by Student's *t* test (* $P < 0.05$; ** $P < 0.01$; *** $P < 0.001$).

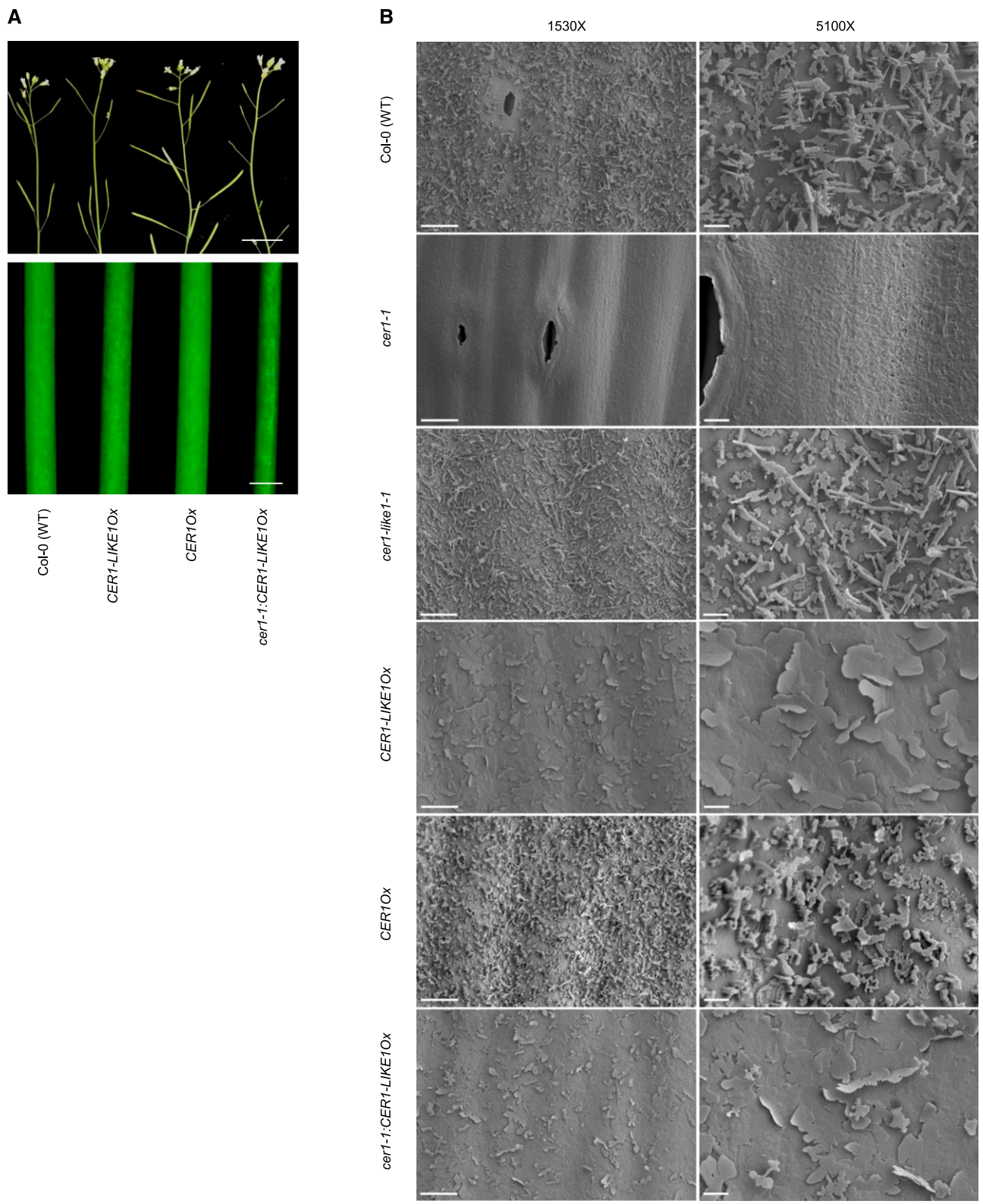


Figure 7. Analysis of epicuticular wax crystals. A, Stems from 6-week-old plants of *CER1-LIKE1Ox* and *cer1-1:CER1-LIKE1Ox* lines showing glossy phenotype compared to nonglossy wild-type (*Col-0*) and *CER1Ox* stems (top, scale bar, 1 cm; bottom, scale bar, 1 mm). B, Epicuticular wax crystals on Arabidopsis wild-type (*Col-0*), *cer1-1*, *cer1-like1*, *CER1-LIKE1Ox*, *CER1Ox*, and *cer1-1:CER1-LIKE1Ox* stem surfaces detected by cryoscanning electron microscopy at 1,530 \times magnification (left, scale bars = 10 μ m) and 5,100 \times magnification (right, scale bar = 2 μ m).

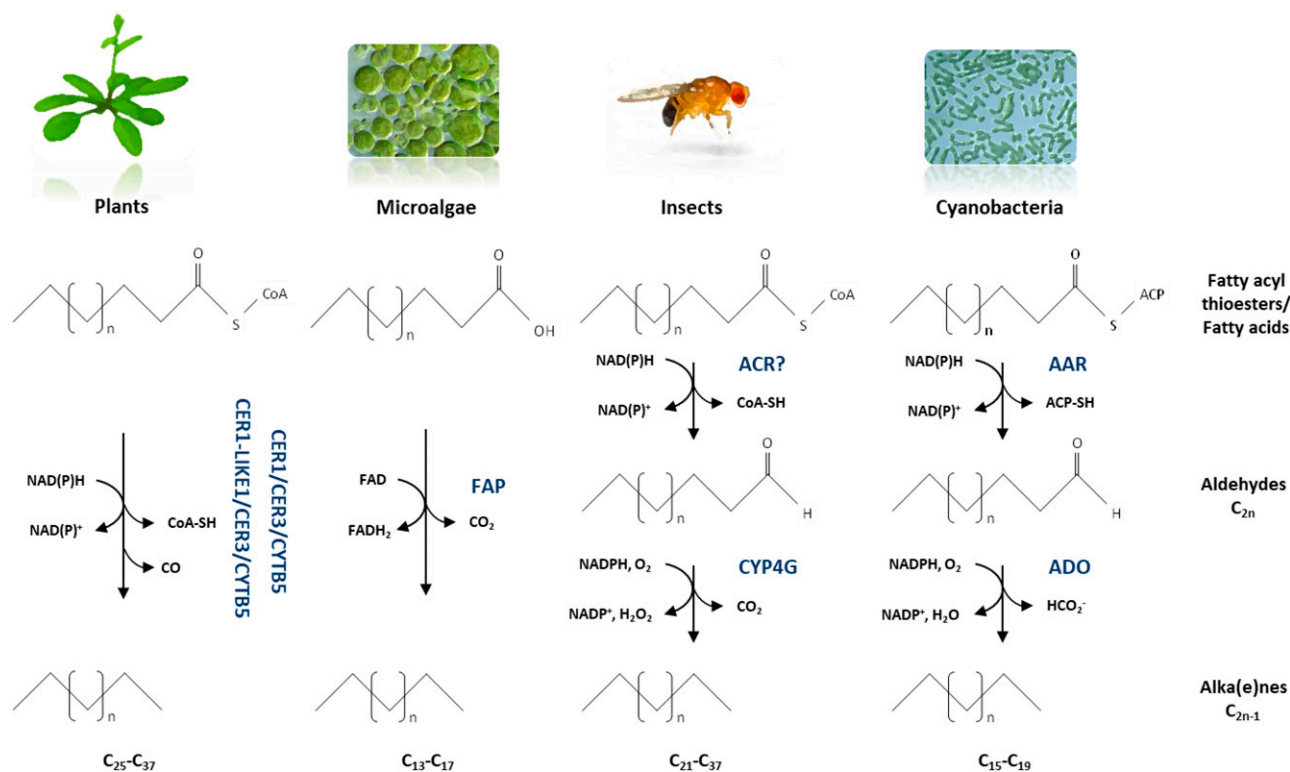


Figure 8. Biochemical models of alkane-forming enzymes in plants, microalgae, insects, and cyanobacteria. The results obtained in this study lead us to propose that in plants, several enzymatic complexes catalyze the conversion of the broad range of VLC-acyl-CoAs to VLC-alkanes. In microalgae, free fatty acids are decarboxylated into alka(e)nes by a unique soluble fatty acid photodecarboxylase (FAP) in the presence of FAD. In insects, VLC-acyl-CoAs are first reduced by an acyl-CoA reductase (ACR) into VLC-aldehydes that are decarboxylated by a cytochrome P450 oxidative decarbonylase (CYP4G). In cyanobacteria, acyl-ACPs are reduced into aldehydes by an acyl-ACP reductase (AAR) that are deformylated by an aldehyde deformylating oxygenase (ADO). ACP, acyl carrier protein; FAD, flavin adenine dinucleotide.

(Shepherd and Wynne Griffiths, 2006). However, our results suggest that the tight balance in *n*-alkane chain length is essential for the correct microstructure of epicuticular waxes. We show that the ectopic expression of *CER1-LIKE1* in stems of both *cer1-1:CER1-LIKE1Ox* and *CER1-LIKE1Ox* lines does not change the overall amount of *n*-alkanes compared to that in wild type but, instead, causes changes in the *n*-alkane profiles, with a higher accumulation of 25 and 27 carbon compounds. These modifications in the chain-length profile of *n*-alkanes prevented the correct crystallization of the epicuticular waxes, which mostly accumulated as large platelets, with occasional polygonal rodlets, arising from an amorphous layer in lines overexpressing *CER1-LIKE1* compared to the typical mixture of platelets, joint-plates, and polygonal rodlets at the surface of wild-type stems. A similar phenotype was already observed by ectopically expressing the *CER2-LIKE1* (also named *CER26*) gene in *Arabidopsis* transgenic plants (Pascal et al., 2013; Haslam et al., 2015). *CER2-LIKE1* is exclusively expressed in the leaves; however, ectopic expression of this gene allows the synthesis of VLCFAs with more than 30 carbon atoms in *Arabidopsis* stems. In these

transgenic plants, a decrease in the amount of non-acosane is accompanied by an increase of *n*-alkanes with 31 and 33 carbon atoms, which are normally found at very low level in stem waxes. Despite the total wax amount being close to that of wild-type stems, this modification of the *n*-alkane profile toward longer chains also impaired the crystallization of the waxes, which instead of crystals formed an amorphous layer at the stem surface. Another example of the critical importance of wax composition for crystal structure is the inactivation of the fatty acyl reductase *CER4/FAR3* (Rowland et al., 2006). The *Arabidopsis cer4* mutant shows a major reduction of primary *n*-alcohols and wax esters in stem epicuticular waxes; however, the total wax load is unchanged due to an increase of the content in compounds produced by the alkane-forming pathway. Nevertheless, the modification of the wax composition in the *cer4* mutant abolished the crystallization of the waxes at the surface of the stems. It therefore seems that the equilibrium of compounds in terms of type of molecules but also in terms of chain lengths is crucial for the formation of wax crystals on the surface of epidermal cells.

Physiological Importance of Cuticular *n*-Alkanes

The specific role of most wax components in cuticle functions during environmental or developmental processes remains largely unknown. Because of the structure of the cuticle, which consists of several embedded and interconnected aliphatic layers, most of the components probably act synergistically in various mechanisms. At present, *n*-alkanes, which are the major wax compounds in *Arabidopsis* and many other species, are one of the few wax components with an established specific contribution in cuticle properties. In *Arabidopsis*, water deprivation and osmotic stress treatments cause an accumulation of *n*-alkanes that, in turn, was associated with plant resistance to drought (Kosma et al., 2009). Moreover, the exhaustive wax analyses of *CER1*-overexpressing lines in various species, including *Arabidopsis*, rice (*Oryza sativa*), and cucumber (*Cucumis sativus*), established a tight correlation between the accumulation of the VLC-*n*-alkanes and the reduction of cuticle permeability, leading to a better plant resistance to water stress (Bourdenx et al., 2011; Zhou et al., 2013; Wang et al., 2015b), thus demonstrating the fundamental role of *n*-alkanes in plant response to environmental stresses.

The high abundance of *CER1-LIKE1* and *CER1* transcripts in flowers in general and in specific flower organs in particular further suggests that the broad chain-length range of cuticular *n*-alkanes produced by *CER1* and *CER1-LIKE1* has important roles in flower physiology and functions beyond the control of non-stomatal water loss. For instance, the *cer1* and *cer3* mutants are male sterile in low humidity but normally fertile in high-humidity conditions (Aarts et al., 1995; Chen et al., 2003; Kurata et al., 2003). In these mutants, the pollen grain surface is altered and the pollen grains fail to rehydrate onto the stigma, suggesting that *n*-alkanes are essential for the integrity of the pollen wall and that the activity of both *CER1* and *CER3* is fundamental to maintain pollen fertility. However, because *CER1-LIKE1* is not expressed in tapetum cells of the anthers, unlike *CER1*, *cer1-like1* mutants did not show any conditional sterility phenotype.

Our results here show that *CER1* and *CER1-LIKE1* (1) have specific expression patterns in flowers, (2) have different substrate specificities and (3) modulate the chain-length profile in *n*-alkanes, which influences wax crystallization processes. Therefore, we propose that the expression of *CER1* and *CER1-LIKE1* specifies both a differential composition of *n*-alkanes and a specific wax crystallization on distinct flower organs. The observation of different crystal microstructures at the surface of flower organs (Bernard and Joubès, 2013; Oshima et al., 2013) supports our hypothesis and raises the question of the functional relevance of such specific patterns of wax crystals in flowers. One possible function of wax crystals is to delimit organ boundaries during flower development and growth (Ingram and Nawrath, 2017). Several cutin mutants show a floral organ fusion phenotype while conserving an intact

epidermal cell layer, suggesting that a proper cuticle is required for the formation and separation of flower organs. Among *Arabidopsis* wax mutants, only *cer3* shows floral organ fusions (Chen et al., 2003; Kurata et al., 2003). Given that cutin synthesis is not impaired in the *cer3* mutant (Rowland et al., 2007), this phenotype suggests that products of the alkane-forming pathway may participate in the prevention of organ fusions. However, compared to the *cer3* mutant (*CER3* is encoded by a single gene in *Arabidopsis*), *cer1-1* and *cer1-like1-1* mutants do not show any flower organ fusions, most likely because of their partial functional redundancy in flower organs. Another possible role of wax crystals in flower physiology is their implication in a self-cleaning process called the “lotus effect” (Barthlott and Neinhuis, 1997). Wax microstructures at the plant surface trigger water repelling, limiting the deposition of dust, pollutants, or pathogen spores, and rendering plant surfaces inappropriate for microorganism colonization. Alternatively, wax crystals at the surface of flower organs may contribute to plant reproduction by participating in the chemical or visual attraction of pollinators; yet, at this time, this aspect is largely unexplored.

The specific function of cuticular *n*-alkanes and how they contribute to the physiological function and physical properties of the cuticular wax mixture remain unclear. Future physicochemical studies of reconstituted wax microenvironments might help in understanding the exact roles of particular wax constituents in the formation of crystals, the mechanisms of crystal formation, as well as the relevance of particular crystal configurations in plant physiology.

MATERIALS AND METHODS

Plant Material and Growth Conditions

Arabidopsis (*Arabidopsis thaliana*, ecotype Columbia-0) was used in all experiments. The following T-DNA or transposon insertion lines were obtained from the *Arabidopsis* Biological Resource Center (www.arabidopsis.org): SALK_008544 (*cer1-1*) and SM_3_23790/CS112237 (*cer1-like1-1*). *Arabidopsis* plants were grown under controlled conditions as previously described (Joubès et al., 2008). For subcellular localization studies, *Nicotiana benthamiana* plants cultivated in controlled conditions (16-h light photoperiod, 25°C) were analyzed 2 d after agroinfiltration as previously described (Perraki et al., 2012).

DNA, RNA, and cDNA Preparation and RT-qPCR Analysis

Genomic DNA was extracted from *Arabidopsis* leaves with the DNeasy Plant kit (Qiagen) and RNA from *Arabidopsis* tissues or yeast cells with the RNeasy Plant mini kit (Qiagen). Purified RNA was treated with DNase I using a DNA-free kit (Ambion, Austin, TX). First-strand complementary DNA (cDNA) was prepared from 500 ng of total RNA with the Superscript RT II kit (Invitrogen) and oligo(dT)₁₈ according to the manufacturer's instructions. RT-qPCR amplification was performed as previously described (Pascal et al., 2013). Semiquantitative RT-PCR analysis and PCR on genomic DNA were performed using Q5 High-Fidelity DNA Polymerase (New England Biolabs). PCR amplifications were performed with gene-specific primers listed in Supplemental Table S1.

DNA Constructs and Transgenic Plants

Promoter sequences and open reading frames (ORFs) were amplified from *Arabidopsis* genomic DNA and from cDNA, respectively, using primers listed in

Supplemental Table S1. The corresponding PCR fragments were inserted into the pDONR221 ENTRY vector using the GATEWAY recombinational cloning technology (Invitrogen) and subsequently transferred into the pKGWFS7, pK7WG2D, pH7WG2D, pK7WGY2, and pH7WGR2 DESTINATION vectors (Karimi et al., 2002) by using LR clonase II. DNA constructs transferred into the *Agrobacterium tumefaciens* GV3101 strain were used for transient expression in *N. benthamiana* leaves (Perraki et al., 2012). For the *CER1-LIKE1* promoter-GUS reporter gene fusion, an 1,106-bp fragment of *CER1-LIKE1* upstream sequence, including the first three codons, was amplified by PCR using BAC T7I23 as template. The forward and reverse primers contained *SalI* and *BamHI* recognition sites, respectively (Supplemental Table S1). The amplified products were digested with *SalI* and *BamHI* and inserted between the corresponding sites of pBI101 (Clontech), thereby fusing the first three codons from the *CER1-LIKE1* coding region in frame with the coding region of the *GUS* gene. DNA constructs were transferred into the *Agrobacterium tumefaciens* C58C1Rif^R strain harboring the plasmid pMP90. The transformed *Agrobacterium* strain was then used to generate stably transformed *Arabidopsis* plants using the floral-dip transformation method (Clough and Bent, 1998). Histochemical GUS analyses were performed as described (Joubès et al., 2008).

For interaction analyses in yeast, *CER1-LIKE1*, *CER1*, *CER3*, and *CYTB5s* ORFs were amplified by PCR using *SfiI* restriction-site-containing primers listed in Supplemental Table S1, with subsequent orientation-specific cloning of *CER1-LIKE1* into the pBT3N bait vector and *CER1-LIKE1*, *CER1*, *CER3*, and *CYTB5s* into the pPR3N prey vector as previously described (Bernard et al., 2012). For heterologous expression in yeast, the ORFs introduced into the pDONR221 ENTRY vector were transferred into yeast expression vectors as summarized in Supplemental Table S2. Site-directed mutagenesis of the ORFs was performed as previously described (Bernard et al., 2012). His 146 codon of *CER1* and *CER1-LIKE1* were replaced by the Ala codon GCT. Primers used for generation of mutation-containing fragments are listed in Supplemental Table S1. *SUR4-F262A/K266L* inserted in the p416 MET25-FLAG3 yeast expression vector was used as previously described (Denic and Weissman, 2007; Bernard et al., 2012).

Western Blotting

Polyacrylamide gels were cast using the TGX Stain-Free FastCast premixed acrylamide solution manufactured by Bio-Rad. After gel activation, total proteins were visualized using Stain free technology with a ChemiDoc MP imaging system (Bio-Rad). For western blotting, mouse anti-MYC-Tag primary antibodies (dilution 1/3,000; Cell Signaling Technology, 9B11) and goat anti-mouse immunoglobulin G-horseradish peroxidase conjugate secondary antibodies (dilution 1/3,000; Bio-Rad, 1721011) were used. Pictures were acquired using a ChemiDoc MP imaging system (Bio-Rad).

Interaction Analyses

Split ubiquitin analysis was performed using the yeast two-hybrid system from DUALmembrane system (Dualsystems Biotech AG) as previously described (Bernard et al., 2012). The *Saccharomyces cerevisiae* strain THY.AP4 [*MATa ura3 leu2 lexA::lacZ::trp1 lexA::HIS3 lexA::ADE2*] was cotransformed with pBT3N:CER1-LIKE1 and pPR3N:PREY or pPR3N empty vector as a negative control by a poly-ethylene glycol/lithium acetate protocol (Ausubel et al., 1995). Transformants were selected on media lacking Trp and Leu and interactions were assayed on media lacking His, Trp, and Leu supplemented with 0.8 mM of 3-amino-1,2,4-triazole or on media additionally lacking adenine. To measure β -galactosidase activity of lacZ with X-gal, cells were grown on media lacking Trp and Leu and then covered with X-gal-agarose buffer (0.5% [w/v] agarose, 0.5M phosphate buffer pH 7.0, 0.002% [w/v] X-gal) and incubated at 37°C for 10 min.

Heterologous Expression in Yeast

S. cerevisiae strain INVSc1 [*MATa his3 Δ 1 leu2 trp1-289 ura3-52*] cells were transformed with different combinations of constructs and grown on minimal medium lacking appropriate amino acids as indicated in Supplemental Table S2. For fatty acyl chain analyses, yeasts were grown in 5 mL of appropriate liquid minimal medium supplemented with 2% Gal (w/v). Yeast cells grown for 1 week at 30°C were pelleted and washed in 2 mL of 2.5% (w/v) NaCl. Fatty acid methyl esters were obtained by transmethylation at 85°C for 1 h. For this, yeast cell pellets were resuspended in 1 mL 0.5 M sulphuric acid in methanol

containing 2% (v/v) dimethoxypropane and 50 μ g of heptadecanoic acid (C17:0) and 10 μ g of docosane (C22 alkane) as internal standards. After cooling, 2 mL of 2.5% (w/v) NaCl was added, and fatty acyl chains, including alkanes, were extracted in 2 mL of hexane. Extracts were then dried under a gentle stream of nitrogen. Samples were dissolved in 100 μ L of hexane and analyzed by gas chromatography-mass spectrometry as previously described (Domergue et al., 2010). For TLC analysis, about 2,000 OD₆₀₀ units were used to prepare fatty acid methyl esters. The alkane fraction was separated from the extracts by TLC on silica gel plates (20 \times 20 cm; Merck) using hexane as the mobile phase, then scraped off and extracted in chloroform, concentrated and analyzed by gas chromatography with flame-ionization detection as well as a gas chromatography-mass spectrometry as previously described (Domergue et al., 2010).

Cuticular Wax Analysis

Epicuticular waxes were extracted from leaves and stems by immersing tissues for 30 s in chloroform containing docosane (C22 alkane) as internal standard. Extracts were derivatized and analyzed as described (Bourdenx et al., 2011). For analysis of epicuticular wax crystal morphology on *Arabidopsis* stem surfaces, segments from the apical part of the stem were mounted onto stubs and examined using cryoscanning electron microscopy (Zeiss Gemini SEM 300, 3 kV).

Confocal Microscopy

Live imaging was performed using a Leica SP5 confocal laser-scanning microscopy system (Leica, Wetzlar, Germany) equipped with Argon, DPSS, He-Ne lasers, hybrid detectors, and 63 \times oil-immersion objective. Two days post-agroinfiltration, *N. benthamiana* leaf samples were gently transferred between a glass slide and a coverslip in a drop of water. YFP and RFP fluorescence were observed using excitation wavelengths of 488 and 561, and their fluorescence emission was collected at 490 to 540 nm and 575 to 610 nm, respectively. Colocalization images were taken using sequential scanning between frames. Experiments were performed using strictly identical confocal acquisition parameters (e.g. laser power, gain, zoom factor, resolution, and emission wavelengths reception), with detector settings optimized for low background and no pixel saturation.

Accession Numbers

Sequence data from this article can be found in the Arabidopsis Genome Initiative or GenBank/EMBL databases under the following accession numbers: *CER1-LIKE1*, At1g02190; *CER1*, At1g02205; *CER3*, At5g57800; *CYTB5-B*, At2g32720; *Actin2*, At1g49240; *eIF4A-1*, At3g13920; *EF-1a*, At5g60390; *UBQ10*, At4g05320; *PP2A*, At1g13320; *ACT1*, YFL039C.

Supplemental Data

The following supplemental materials are available.

Supplemental Table S1. Primers used for PCR cloning and PCR analysis

Supplemental Table S2. Transgenic yeasts

ACKNOWLEDGMENTS

We thank the Arabidopsis Biological Resource Center for providing the sequence-indexed Arabidopsis insertion lines. Cryoscanning electron and confocal microscopy analyses were performed at the Bordeaux Imaging Center (<http://www.bic.u-bordeaux.fr/>). Lipid analyses were carried out at Metabome facility of Bordeaux (<https://cgfb.u-bordeaux.fr/>).

Received September 4, 2018; accepted November 26, 2018; published December 4, 2018.

LITERATURE CITED

Aarts MG, Keijzer CJ, Stiekema WJ, Pereira A (1995) Molecular characterization of the *CER1* gene of *Arabidopsis* involved in epicuticular wax biosynthesis and pollen fertility. *Plant Cell* 7: 2115–2127

- Aarts MG, Hodge R, Kalantidis K, Florack D, Wilson ZA, Mulligan BJ, Stiekema WJ, Scott R, Pereira A (1997) The Arabidopsis MALE STERILITY 2 protein shares similarity with reductases in elongation/condensation complexes. *Plant J* **12**: 615–623
- Ausubel FM, Brent R, Kingston RE, Moore DD, Seidman JG, Smith JA, Struhl K, Albricht LM, Coen DM, Varki A (1995) *Current Protocols in Molecular Biology*. John Wiley & Sons, New York
- Bach L, Michaelson LV, Haslam R, Bellec Y, Gissot L, Marion J, Da Costa M, Boutin JP, Miquel M, Tellier F, et al (2008) The very-long-chain hydroxy fatty acyl-CoA dehydratase PASTICCINO2 is essential and limiting for plant development. *Proc Natl Acad Sci USA* **105**: 14727–14731
- Barthlott W, Neinhuis C (1997) Purity of the sacred lotus, or escape from contamination in biological surfaces. *Planta* **202**: 1–8
- Beaudoin F, Wu X, Li F, Haslam RP, Markham JE, Zheng H, Napier JA, Kunst L (2009) Functional characterization of the Arabidopsis β -ketoacyl-coenzyme A reductase candidates of the fatty acid elongase. *Plant Physiol* **150**: 1174–1191
- Bernard A, Joubès J (2013) Arabidopsis cuticular waxes: Advances in regulation, synthesis, export and regulation. *Prog Lipid Res* **52**: 110–129
- Bernard A, Domergue F, Pascal S, Jetter R, Renne C, Faure JD, Haslam RP, Napier JA, Lessire R, Joubès J (2012) Reconstitution of plant alkane biosynthesis in yeast demonstrates that Arabidopsis ECERIFERUM1 and ECERIFERUM3 are core components of a very-long-chain alkane synthesis complex. *Plant Cell* **24**: 3106–3118
- Bourdenx B, Bernard A, Domergue F, Pascal S, Léger A, Roby D, Pervent M, Vile D, Haslam RP, Napier JA, et al (2011) Overexpression of Arabidopsis ECERIFERUM1 promotes wax very-long-chain alkane biosynthesis and influences plant response to biotic and abiotic stresses. *Plant Physiol* **156**: 29–45
- Buschhaus C, Jetter R (2011) Composition differences between epicuticular and intracuticular wax substructures: How do plants seal their epidermal surfaces? *J Exp Bot* **62**: 841–853
- Buschhaus C, Jetter R (2012) Composition and physiological function of the wax layers coating Arabidopsis leaves: β -amyryn negatively affects the intracuticular water barrier. *Plant Physiol* **160**: 1120–1129
- Busta L, Jetter R (2017) Structure and biosynthesis of branched wax compounds on wild type and wax biosynthesis mutants of *Arabidopsis thaliana*. *Plant Cell Physiol* **58**: 1059–1074
- Busta L, Hegebarth D, Kroc E, Jetter R (2017) Changes in cuticular wax coverage and composition on developing Arabidopsis leaves are influenced by wax biosynthesis gene expression levels and trichome density. *Planta* **245**: 297–311
- Chen W, Yu XH, Zhang K, Shi J, De Oliveira S, Schreiber L, Shanklin J, Zhang D (2011) *Male Sterile2* encodes a plastid-localized fatty acyl carrier protein reductase required for pollen exine development in Arabidopsis. *Plant Physiol* **157**: 842–853
- Chen X, Goodwin SM, Boroff VL, Liu X, Jenks MA (2003) Cloning and characterization of the WAX2 gene of *Arabidopsis* involved in cuticle membrane and wax production. *Plant Cell* **15**: 1170–1185
- Clough SJ, Bent AF (1998) Floral dip: A simplified method for Agrobacterium-mediated transformation of *Arabidopsis thaliana*. *Plant J* **16**: 735–743
- Denic V, Weissman JS (2007) A molecular caliper mechanism for determining very long-chain fatty acid length. *Cell* **130**: 663–677
- Domergue F, Vishwanath SJ, Joubès J, Ono J, Lee JA, Bourdon M, Alhattab R, Lowe C, Pascal S, Lessire R, et al (2010) Three Arabidopsis fatty acyl-coenzyme A reductases, FAR1, FAR4, and FAR5, generate primary fatty alcohols associated with suberin deposition. *Plant Physiol* **153**: 1539–1554
- Fich EA, Segerson NA, Rose JK (2016) The plant polyester cutin: Biosynthesis, structure, and biological roles. *Annu Rev Plant Biol* **67**: 207–233
- Fu WJ, Chi Z, Ma ZC, Zhou HX, Liu GL, Lee CF, Chi ZM (2015) Hydrocarbons, the advanced biofuels produced by different organisms, the evidence that alkanes in petroleum can be renewable. *Appl Microbiol Biotechnol* **99**: 7481–7494
- Gorb EV, Gorb SN (2017) Anti-adhesive effects of plant wax coverage on insect attachment. *J Exp Bot* **68**: 5323–5337
- Greer S, Wen M, Bird D, Wu X, Samuels L, Kunst L, Jetter R (2007) The cytochrome P450 enzyme CYP96A15 is the midchain alkane hydroxylase responsible for formation of secondary alcohols and ketones in stem cuticular wax of Arabidopsis. *Plant Physiol* **145**: 653–667
- Guo HS, Zhang YM, Sun XQ, Li MM, Hang YY, Xue JY (2016) Evolution of the KCS gene family in plants: the history of gene duplication, sub/neofunctionalization and redundancy. *Mol Genet Genomics* **291**: 739–752
- Haslam TM, Kunst L (2013) Extending the story of very-long-chain fatty acid elongation. *Plant Sci* **210**: 93–107
- Haslam TM, Haslam R, Thoraval D, Pascal S, Delude C, Domergue F, Fernández AM, Beaudoin F, Napier JA, Kunst L, et al (2015) ECERIFERUM2-LIKE proteins have unique biochemical and physiological functions in very-long-chain fatty acid elongation. *Plant Physiol* **167**: 682–692
- Hegebarth D, Buschhaus C, Joubès J, Thoraval D, Bird D, Jetter R (2017) Arabidopsis ketoacyl-CoA synthase 16 (KCS16) forms C₃₆/C₃₈ acyl precursors for leaf trichome and pavement surface wax. *Plant Cell Environ* **40**: 1761–1776
- Ingram G, Nawrath C (2017) The roles of the cuticle in plant development: Organ adhesions and beyond. *J Exp Bot* **68**: 5307–5321
- Jenks MA, Tuttle HA, Eigenbrode SD, Feldmann KA (1995) Leaf epicuticular waxes of the *eceriferum* mutants in Arabidopsis. *Plant Physiol* **108**: 369–377
- Jiménez-Díaz L, Caballero A, Pérez-Hernández N, Segura A (2017) Microbial alkane production for jet fuel industry: Motivation, state of the art and perspectives. *Microb Biotechnol* **10**: 103–124
- Joubès J, Raffaele B, Bourdenx B, Garcia C, Laroche-Traineau J, Moreau P, Domergue F, Lessire R (2008) The VLCFA elongase gene family in *Arabidopsis thaliana*: Phylogenetic analysis, 3D modelling and expression profiling. *Plant Mol Biol* **67**: 547–566
- Karimi M, Inzé D, Depicker A (2002) GATEWAY vectors for Agrobacterium-mediated plant transformation. *Trends Plant Sci* **7**: 193–195
- Kosma DK, Bourdenx B, Bernard A, Parsons EP, Lü S, Joubès J, Jenks MA (2009) The impact of water deficiency on leaf cuticle lipids of Arabidopsis. *Plant Physiol* **151**: 1918–1929
- Kunst L, Samuels AL (2003) Biosynthesis and secretion of plant cuticular wax. *Prog Lipid Res* **42**: 51–80
- Kurata T, Kawabata-Awai C, Sakuradani E, Shimizu S, Okada K, Wada T (2003) The YORE-YORE gene regulates multiple aspects of epidermal cell differentiation in Arabidopsis. *Plant J* **36**: 55–66
- Lee SB, Suh MC (2015) Advances in the understanding of cuticular waxes in *Arabidopsis thaliana* and crop species. *Plant Cell Rep* **34**: 557–572
- Li F, Wu X, Lam P, Bird D, Zheng H, Samuels L, Jetter R, Kunst L (2008) Identification of the wax ester synthase/acyl-coenzyme A: Diacylglycerol acyltransferase WSD1 required for stem wax ester biosynthesis in Arabidopsis. *Plant Physiol* **148**: 97–107
- Martin LB, Rose JK (2014) There's more than one way to skin a fruit: Formation and functions of fruit cuticles. *J Exp Bot* **65**: 4639–4651
- Oshima Y, Shikata M, Koyama T, Ohtsubo N, Mitsuda N, Ohme-Takagi M (2013) MIXTA-like transcription factors and WAX INDUCER1/SHINE1 coordinately regulate cuticle development in *Arabidopsis* and *Torenia fournieri*. *Plant Cell* **25**: 1609–1624
- Pascal S, Bernard A, Sorel M, Pervent M, Vile D, Haslam RP, Napier JA, Lessire R, Domergue F, Joubès J (2013) The Arabidopsis *cer26* mutant, like the *cer2* mutant, is specifically affected in the very long chain fatty acid elongation process. *Plant J* **73**: 733–746
- Perraki A, Cacas JL, Crowet JM, Lins L, Castroviejo M, German-Retana S, Mongrand S, Raffaele S (2012) Plasma membrane localization of Solanum tuberosum remorin from group 1, homolog 3 is mediated by conformational changes in a novel C-terminal anchor and required for the restriction of potato virus X movement. *Plant Physiol* **160**: 624–637
- Qiu Y, Tittiger C, Wicker-Thomas C, Le Goff G, Young S, Wajnberg E, Fricaux T, Taquet N, Blomquist GJ, Feyereisen R (2012) An insect-specific P450 oxidative decarboxylase for cuticular hydrocarbon biosynthesis. *Proc Natl Acad Sci USA* **109**: 14858–14863
- Rowland O, Domergue F (2012) Plant fatty acyl reductases: enzymes generating fatty alcohols for protective layers with potential for industrial applications. *Plant Sci* **193–194**: 28–38
- Rowland O, Zheng H, Hepworth SR, Lam P, Jetter R, Kunst L (2006) *CER4* encodes an alcohol-forming fatty acyl-coenzyme A reductase involved in cuticular wax production in Arabidopsis. *Plant Physiol* **142**: 866–877
- Rowland O, Lee R, Franke R, Schreiber L, Kunst L (2007) The *CER3* wax biosynthetic gene from *Arabidopsis thaliana* is allelic to *WAX2/YRE/FLP1*. *FEBS Lett* **581**: 3538–3544

- Schirmer A, Rude MA, Li X, Popova E, del Cardayre SB (2010) Microbial biosynthesis of alkanes. *Science* **329**: 559–562
- Shepherd T, Wynne Griffiths D (2006) The effects of stress on plant cuticular waxes. *New Phytol* **171**: 469–499
- Smyth DR, Bowman JL, Meyerowitz EM (1990) Early flower development in *Arabidopsis*. *Plant Cell* **2**: 755–767
- Sorigué D, Légeret B, Cuiné S, Morales P, Mirabella B, Guédeney G, Li-Beisson Y, Jetter R, Peltier G, Beisson F (2016) Microalgae synthesize hydrocarbons from long-chain fatty acids via a light-dependent pathway. *Plant Physiol* **171**: 2393–2405
- Sorigué D, Légeret B, Cuiné S, Blangy S, Moulin S, Billon E, Richaud P, Brugière S, Couté Y, Nurizzo D, et al (2017) An algal photoenzyme converts fatty acids to hydrocarbons. *Science* **357**: 903–907
- Wang W, Liu X, Gai X, Ren J, Liu X, Cai Y, Wang Q, Ren H (2015a) *Cucumis sativus* L. *WAX2* plays a pivotal role in wax biosynthesis, influencing pollen fertility and plant biotic and abiotic stress responses. *Plant Cell Physiol* **56**: 1339–1354
- Wang W, Zhang Y, Xu C, Ren J, Liu X, Black K, Gai X, Wang Q, Ren H (2015b) Cucumber *ECERIFERUM1* (*CsCER1*), which influences the cuticle properties and drought tolerance of cucumber, plays a key role in VLC alkanes biosynthesis. *Plant Mol Biol* **87**: 219–233
- Xue D, Zhang X, Lu X, Chen G, Chen ZH (2017). Molecular and evolutionary mechanisms of cuticular wax for plant drought tolerance. *Front Plant Sci* **8**: 621.
- Zheng H, Rowland O, Kunst L (2005) Disruptions of the *Arabidopsis* Enoyl-CoA reductase gene reveal an essential role for very-long-chain fatty acid synthesis in cell expansion during plant morphogenesis. *Plant Cell* **17**: 1467–1481
- Zhou L, Ni E, Yang J, Zhou H, Liang H, Li J, Jiang D, Wang Z, Liu Z, and Zhuang C (2013). Rice OsGL1-6 is involved in leaf cuticular wax accumulation and drought resistance. *PLoS One* **8**: e65139.
- Ziv C, Zhao Z, Gao YG, Xia Y (2018) Multifunctional roles of plant cuticle during plant-pathogen interactions. *Front Plant Sci* **9**: 1088